Application of Gradient Dose Segmented Analysis as a Treatment Quality Indicator for Patients Undergoing Volumetric Modulated Arc Radiotherapy

by

Christoffel Jacobus van Reenen

Thesis presented in fulfilment of the requirements for the degree of
Master of Science in the Faculty of Medicine and Health Sciences
at Stellenbosch University

Supervisor: Prof Christoph Jan Trauernicht

Co-supervisor: Dr Casey Bojechko

December 2022

“DECLARATION

By submitting this thesis electronically, I declare that the entirety of the work contained therein is my own, original work, that I am the sole author thereof (save to the extent explicitly otherwise stated), that reproduction and publication thereof by Stellenbosch University will not infringe any third party rights and that I have not previously in its entirety or in part submitted it for obtaining any qualification.”

This thesis includes 1 original first-author paper submitted to a peer-reviewed journal. The development, research and writing of the paper was the principal responsibility of myself.

December 2022

Abstract

The gamma analysis metric is a commonly used metric for volumetric modulated arc radiotherapy (VMAT) plan evaluation. The major drawback of this metric is the lack of correlation between gamma passing rates and dose-volume histogram (DVH) values for planning target volumes (PTV). The novel gradient dose segmented analysis (GDSA) metric was developed by Steers et al. to quantify changes in the PTV mean dose (D_{mean}) for patients undergoing VMAT.

In this study, the GDSA metric was applied to 115 head-and-neck cancer patients treated on the Varian Halcyon v2.0 linear accelerator between August 2019 and July 2020 in the Division of Radiation Oncology. The GDSA indicated that a total of 13 patients had received at least one treatment fraction where the PTV Dmean exceeded 3% compared to the first treatment fraction. The kilovoltage cone-beam computed tomography (kV CBCT) images of these patients were analysed to determine the cause.

The maximum predicted change in the PTV D_{mean} was 4.83%. Measurable changes in anterior-posterior and lateral separations were observed for 8 out the 13 patients (62%) where the change in PTV D_{mean} exceeded 3%. The maximum calculated effective separation change diameter was calculated as 3.86 cm. In cases where the change in PTV D_{mean} was less than 3%, no measurable separation changes were observed. The pitch-, roll- and yaw-rotational errors were quantified as the Halcyon treatment couch does not allow for online rotational corrections. The maximum pitch, roll and yaw rotational errors were 3.91º ± 0.89º, 3.07º ± 0.51º and 2.62º ± 0.40º, respectively. The mean errors were 0.9º, 0.45º, and 0.43º, for pitch, roll and yaw, respectively.

The obtained results demonstrated that large deviations in PTV D_{mean} (>3%) were more likely due to change in effective diameter, whereas small deviations in PTV D_{mean} combined with separation changes less than 1 cm, were more likely caused by errors in pitch for long treatment fields. Weight loss during radiotherapy is well documented and proven to be the highest among head-and-neck cancer patients. The GDSA easily be

implemented to identify setup/immobilization errors, as well as aid the department in scheduling new CT scans for patients experiencing continuous weight loss before significant differences in dose delivery occur.

Opsomming

Die gamma-analise word oor die algemeen as ‘n plan evaluasie metode vir Volumetriese Gemoduleerde Boogterapie (VGBT, “VMAT”) gebruik. Die grootste nadeel daarvan is die gebrek aan korrelasie tussen die gamma-analise en beplannings-teikenvolumes (BTV) van dosis-volume histogramme (DVH). *Steers et al.* het ‘n nuwe metode ontwikkel om hierdie probleem te oorkom. Die gesegmenteerde-dosis-gradiënt-analise (GDGA) kan direk gebruik word om die gemiddelde dosis-verandering in die BTV te bereken vir pasiënte wat VGBT ondergaan.

Die GDGA is retrospektief op 115 kop-en-nek kanker pasiënte toegepas wat tussen Augustus 2019 en Julie 2020 op die Varian Halcyon v2.0 lineêre versneller behandel is. Die GDGA analise het getoon dat ‘n totaal van 13 pasiënte ten minste een fraksie van radioterapie ontvang het, waar die gemiddelde dosis-verandering in die BTV hoër as 3% is vergelyke met die eerste behandelingsfraksie. Die Keëlstraal-rekenaartomografiese beelde van hierdie pasiënte is analiseer om die oorsprong van hierdie dosis-veranderinge te ondersoek.

Die maksimum gemiddelde dosis-verandering in die BTV was 4.83%. Vir agt uit die dertien pasiënte (62%) was daar merkbare veranderinge in hul anterior-posterior en laterale separasies. Die maksimum berekende effektiewe separasie diameter verandering is 3.86 cm. Geen merkbare veranderinge in separasie is bereken vir pasiënte waar die gemiddelde dosis-verandering in die BTV onder 3% is nie. Die Halcyon se pasiënt bed laat nie vir rotasie verstellings toe nie en daarom is die hei, rol en gier foute bereken. Die maksimum hei, rol en gier rotasie foute is onderskeidelik as 3.91º ± 0.89º, 3.07º ± 0.51º en 2.62º ± 0.40º, bereken. Die gemiddelde foute vir hei, rol en gier is onderskeidelik bereken as 0.9º, 0.45º en 0.43º.

Die resultate toon merkbare veranderinge in die pasiënte se effektiewe diameter as die gemiddelde dosis-verandering van die BTV hoër as 3% is. Verder, word klein veranderinge in die gemiddelde dosis-verandering van die BTV tesame met separasie

veranderinge kleiner as 1 cm, in alle waarskynlikheid deur foute in die hei van die pasiënte veroorsaak. Gewigsverlies tydens radioterapie vir kop-en-nek kankers word volledig in die literatuur omskryf. Dit is maklik om die GDGA in praktyk te implementeer om foute in opstelling/immobilisasie en stelselmatige gewigsverlies in pasiënte te monitor voordat merkbare veranderinge in gegewe radioterapie dosisse voorkom.

Acknowledgements

I would like to acknowledge and thank both of my supervisors who made this work possible. Their guidance and advice carried me through all the stages of this project.

I would also like to give special thanks to my partner and my family for their continuous support, encouragement and understanding.

Table of Contents

List of Figures

Chapter 1:

1. Chapter 1 – Introduction

1.1 Background

Globally, cancer is the second leading cause of death and was responsible for an estimated 9.6 million deaths in 2018[1]. Approximately 1 in 6 deaths globally is due to cancer[2]. The World Health Organization also estimates that 70% of deaths from cancer occur in low- and middle-income countries[2].

In South Africa, approximately 107 467 new cancer cases were reported in the year 2018 alone, along with 57 373 cancer deaths[3]. Roughly 61% of these patients will undergo external beam radiation therapy as part of their treatment regime[4]. This treatment makes use of high-energy particles (or photons) generated by linear accelerators which are focused at precise and calculated positions around the patient. External beam radiotherapy damages cells through direct and indirect damages of the genetic material that controls how cells grow and divide. While both normal and cancerous cells are damaged by radiation therapy, the goal is to minimize damage of normal cells, whilst maximizing the damage of cancerous cells for optimal tumour control.

The clinical dose delivery accuracy for radiotherapy is based on evidence (Figure 1-1) for tumour control probability (TCP) and normal tissue complication probability (NTCP) from dose response curves. Generally, the TCP and NTCP overlap on the dose axis such that the dose to the tumour is limited by what can be tolerated by the most at-risk normal tissues. The current recommended tolerance level on accuracy in dose delivery is 3% on the delivered absorbed dose to the patient, to keep TCP within tolerable limits[5].

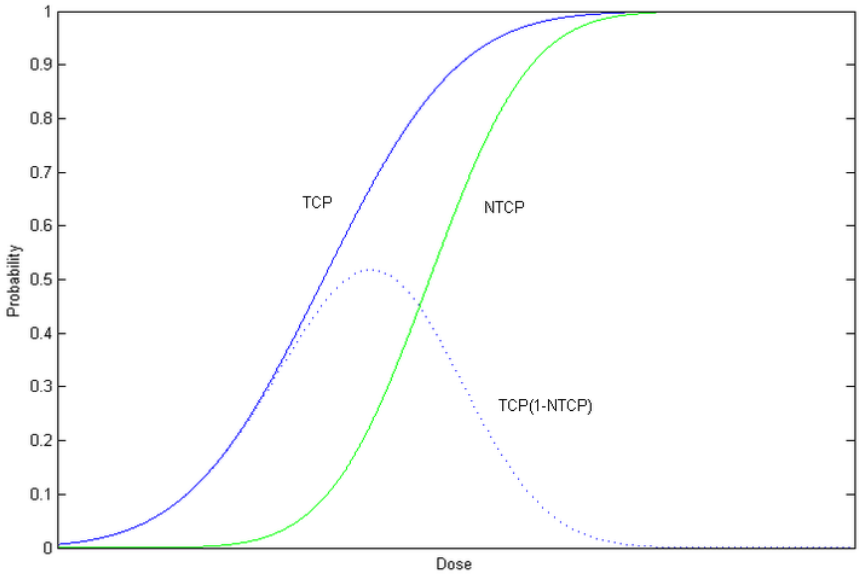

Figure 1-1. A typical dose-response curve showing the tumour control probability (TCP), normal tissue complication probability (NTCP), and the probability for tumour control without normal tissue complications [TCP(1-NTCP)][6].

To comply with the required accuracy in dose delivery, Radiation Oncology departments have dedicated quality assurance programs to ensure that patients receive safe, effective, and high-quality treatments. These quality assurance programmes focus on each individual link in the radiotherapy treatment chain (Figure 1-2).

Figure 1-2. The Radiotherapy treatment chain.

As radiotherapy techniques become more complex, it is difficult to rely on manual checking processes to detect and minimise errors. While most of the processes in the chain can be automated to some extent, patient-specific pre-treatment quality assurance,

mostly referred to as Volumetric Modulated Arc Therapy (VMAT) quality assurance (QA), involves a tedious process of obtaining a physical measurement of the patient's radiotherapy treatment plan to compare to what was planned in the treatment planning system (TPS).

1.1.1 Brief history and evolution of external beam radiotherapy (EBRT)

Radiotherapy has played a significant role in the treatment of cancer for the past 120 years since the initial discovery of x-rays by Wilhelm C. Roentgen in 1895 and the discovery of radioactivity and radium by Antoine H. Becquerel, Pierre Curie and his wife, Marie Skłodowska-Curie, in 1898[7–10].

In the beginning of the 19th century, an increased number of studies reported the use of x-rays and radium in medicine. The next milestone in the field was when a research group proved that head and neck cancers could be cured by fractionated radiotherapy treatments.[8,10] The International Commission on Radiological Protection (ICRP) was established in 1928 to standardise radiation protection guidelines in use around the world[11]. The next decades were characterised by continuous scientific progress to treat patients using radium-based interstitial radiotherapy (brachytherapy) and the development of treatment modalities to treat superficial tumors[8,10].

The modern era of radiotherapy began in the 1950's with the introduction of cobalt teletherapy, megavoltage therapy, the use of proton beams, and the electron linear accelerator. These technologies allowed for the use of deep-penetrating, precisely focused radiation beams without damaging the skin and normal tissue surrounding the tumors[8,12]. These radiotherapy beams were commonly shaped using rectangular high-density jaws in the accelerator head (Figure 1-3). Subsequent improvements were made to shape and control dose distributions to improve normal tissue sparing without sacrificing tumour coverage. Patient-customized Wood's metal/Lipowitz's alloy (commonly known by its trade name, Cerrobend™) blocks were introduced in combination with primary rectangular collimation to shield normal tissues[8,13,14].

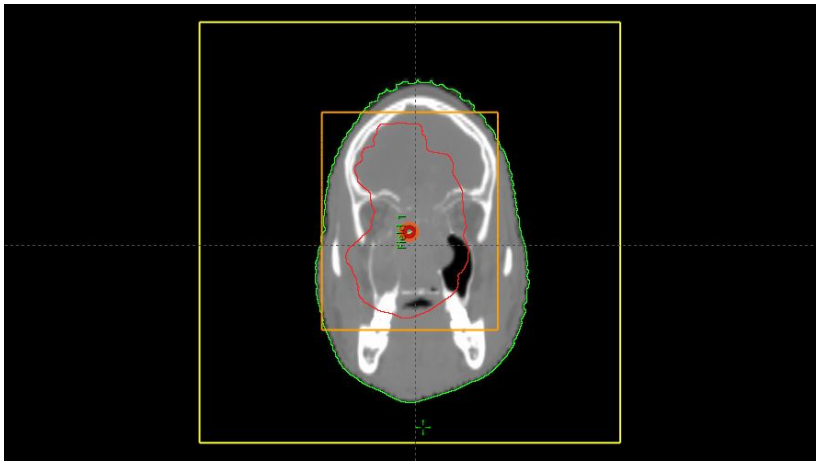

Figure 1-3. An example of a treatment field defined with rectangular primary collimators covering the extent of the Planning Target volume (PTV).

Advances in computer technology enabled the transition from basic two-dimensional planning to 3-D Conformal Radiotherapy (3D-CRT). 3D-CRT makes use of CT images and treatment planning computers to generate 3-D representations of tumour and normal tissue volumes and to visualise dose distributions in 3-D (Figure 1-4). The planning of 3D-CRT makes use of a forward-planning scheme to achieve the required dose distribution[15].

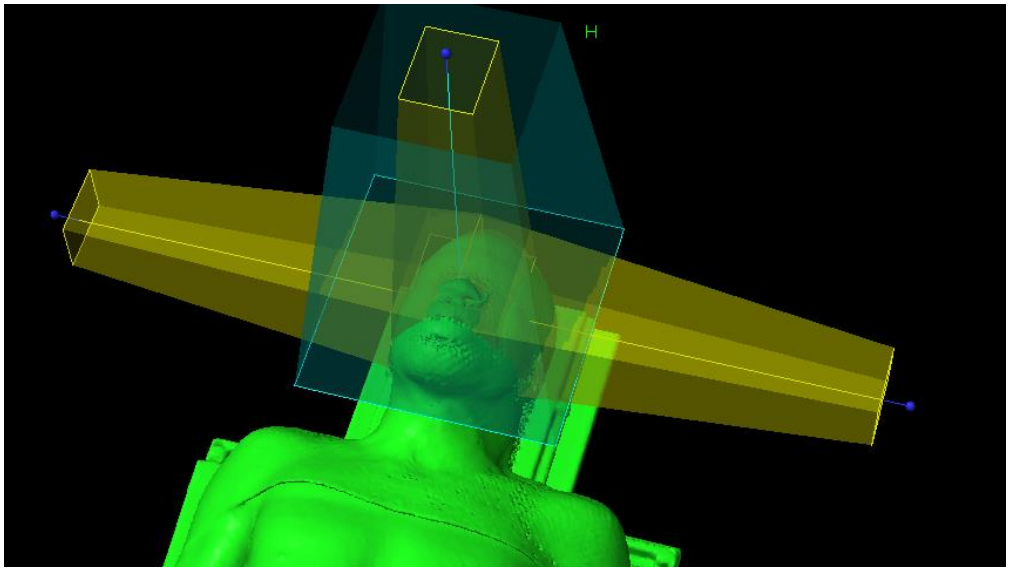

Figure 1-4. An example of a 3D-CRT treatment plan showing static beam orientation.

Multi-leaf collimators (MLCs) were introduced in the 1980's and were in wide-spread use by the 1990's[16,17]. MLC systems contain individually movable leaves, which can block-off parts of the radiation beam (Figure 1-5). Typical MLC designs employ 80 to 160 leaves arranged in leaf-pairs. By controlling and moving these narrow, closely abutting individual leaves, almost any desired field shape can be obtained[13,16,17].

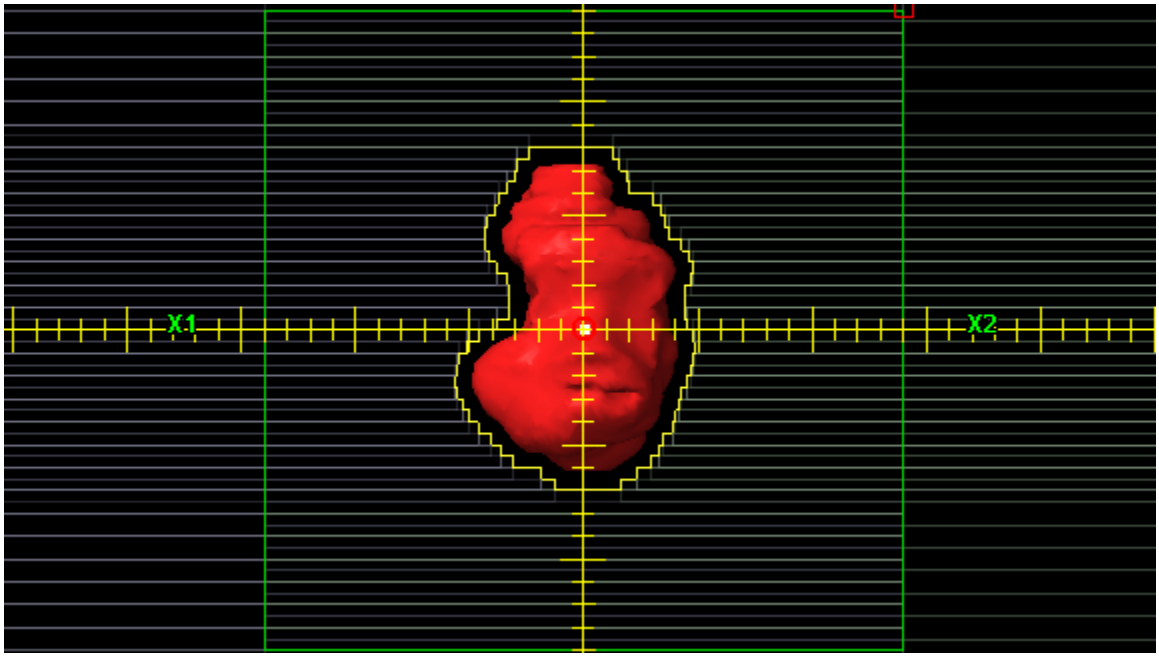

Figure 1-5. Multi-leaf collimators conformed to the Beams-eye-view (BEV) projection of the PTV with a uniform 7 mm margin.

Intensity-modulated radiotherapy (IMRT) was introduced in 1988 after advances were made in computerised treatment planning systems[8,18]. IMRT delivery can be divided into dynamic IMRT and static IMRT (Figure 1-6). In dynamic IMRT, the continuously moving MLCs continuously modulate the beam, whereas in static IMRT, the radiation beam is split up into a subset of smaller MLC segments, and the radiation beam is switched off between the segments[19,20].

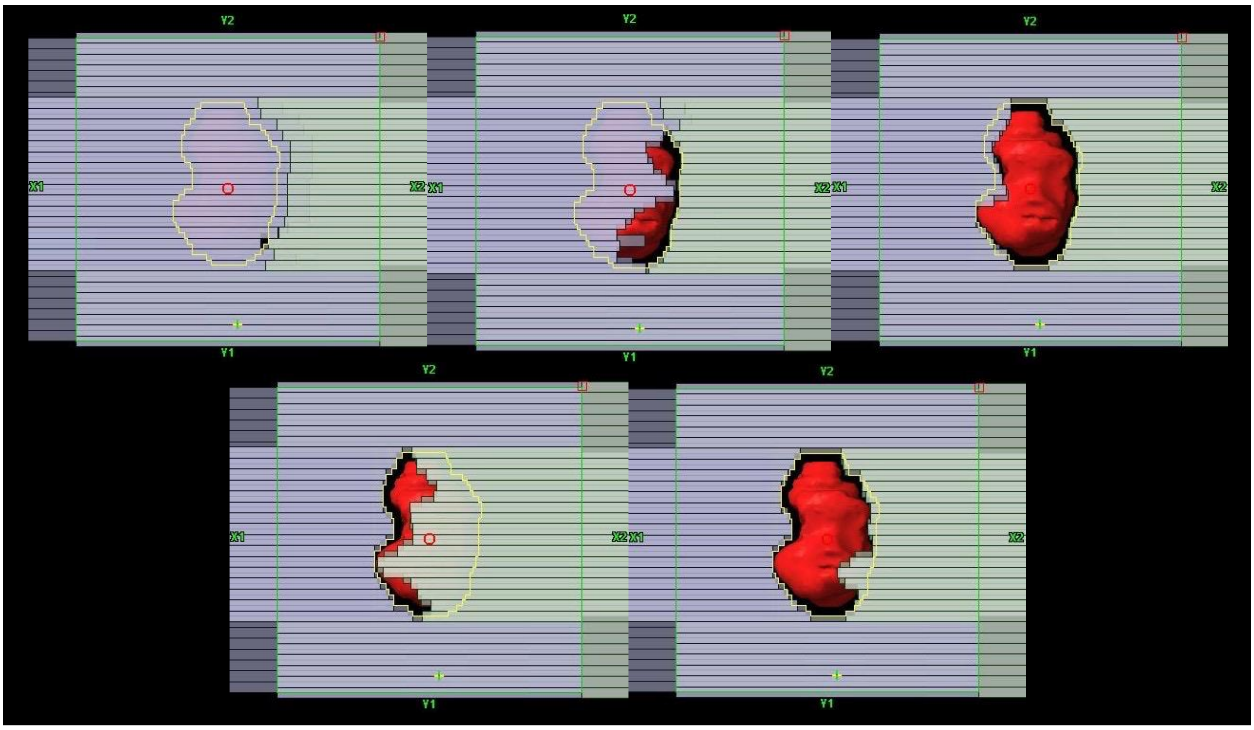

Figure 1-6. BEV showing multiple segments of a sliding window IMRT plan.

After more technological advances in computing power and dose optimization algorithms, VMAT was introduced to speed up the longer delivery times associated with IMRT treatments. In VMAT, one or multiple arcs are used for the treatment, and the delivery technique allows the simultaneous variation in gantry rotation speed, dose rate, and MLC leaf positions[19,20]. VMAT treatment plans are characterised by complex MLC segments generated by dose optimization engines (Figure 1-7).

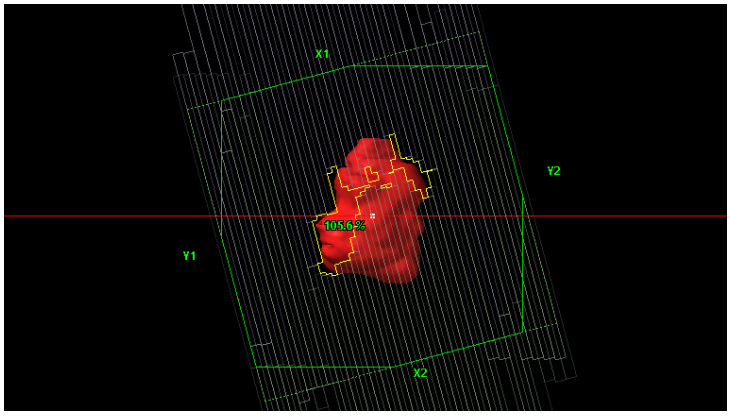

Figure 1-7. BEV showing one segment of an arc of a VMAT treatment plan.

The planning of IMRT and VMAT makes use of an inverse planning scheme, where users define dose objectives, and optimization algorithms attempt to meet these objectives[15].

1.1.2 Current routine practice in VMAT QA

The complexity of radiotherapy treatments increased with the introduction of IMRT and VMAT. The multiple, complex MLC segments introduced more uncertainties in the treatment planning process. Many radiotherapy departments started employing independent monitor unit (MU) check programs to ensure that the expected beam segments summed up to the expected dose[21]. Additionally, medical physicists started to deliver each segment (or arc, in the case of VMAT) of the plan on a measurement device prior to the patient's treatment[22].

GAFchromic film was initially utilised to visualize the dose distribution in 2-D, but it proved to be a tedious process of calibration, scanning and analysis. Many departments also employed the use of ionisation chambers for absolute dose verification[23–27]. The most commonly employed measurement devices are now 2-D ionisation chamber and diode arrays or cylindrical phantoms[28–32]. An increasingly popular technique employs the flat-panel imager, or EPID, equipped on many linear accelerators that facilitates the acquisition of patient-specific pre-treatment measurements[33,34]. Figure 1-8 shows an example of an EPID-based pre-treatment dose distribution measurement of a VMAT arc.

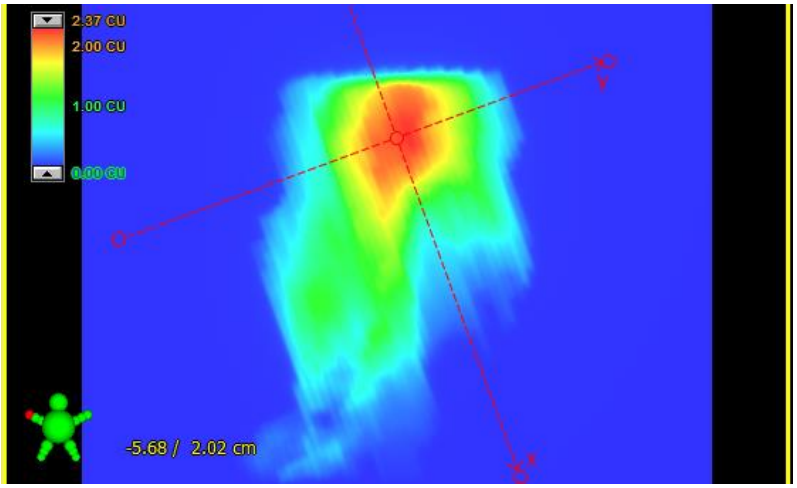

Figure 1-8. The fluence map of a single VMAT arc as measured by an EPID-based system.

1.1.3 Analysis of VMAT QA dose distributions

The gamma-analysis metric was introduced to allow for the relatively quick comparison of the 2-D array or EPID-based measurements with the TPS planned dose distributions. Gamma-analysis was first introduced by Low *et al.*[35] to easily compare calculated (evaluated) and measured (reference) dose distributions. This technique employs the physical separation (distance) as well as the dose difference between dose points, which are normalized by the acceptance criteria: the distance to agreement (DTA) and the dose differences (DD)[36].

The DTA and DD is used to calculate a unitless metric for each point in the evaluated dose distribution. The gamma, γ, is calculated based on finding the minimum line-separation distance for each reference point (Figure 1-2). For each reference point in the dose distribution, calculate against each point in the evaluated distribution:

(i) the distance between reference to evaluated point: $\Delta r(\boldsymbol{r}_R, \boldsymbol{r}_E)$, where $\boldsymbol{r}_R$ is the reference point and $\boldsymbol{r}_E$ is the evaluated point, and

(ii) the dose difference between the reference and evaluated point: $\Delta D(\boldsymbol{r}_R, \boldsymbol{r}_E) = D_E(r_E) - D_R(r_R)$, where $D_E(r_E)$ is the dose at a point in the evaluated dose distribution, r_E, and $D_R(r_R)$ is the reference point dose.

Then for each point in the evaluated distribution, the gamma is calculated using Eq. (1):

$$\Gamma(r_R, r_E) = \sqrt{\frac{\Delta r^2(r_R, r_E)}{\delta r^2} + \frac{\Delta D^2(r_R, r_E)}{\delta D^2}} \quad (1)$$

where δr is the distance difference criterion and δD is the dose difference criterion.

The γ is then taken as the minimum value calculated over all evaluated points as shown in Eq. (2):

$$\gamma(r_R) = \min\{\Gamma(r_R, r_E)\} \forall \{r_E\} \quad (2)$$

In Figure 1-9, the cross is the reference point, and the blue line represents the evaluated dose distribution with the solid circles representing discrete dose points along the line. The δr and δD criteria create an acceptance ellipse around the reference point. The result of Eq. (3) would be $\gamma < 1$ for the reference point, $D_R(r_R), r_R$.

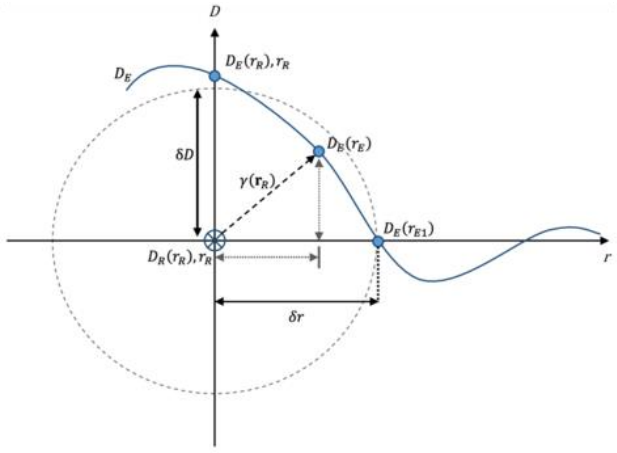

Figure 1-9. Schematic representation of the gamma-analysis method in 1-D[37].

It is considered acceptable to report the passing criteria used for the gamma-analysis in the format $\delta D(\%)/\delta r(mm)$. The most common passing criteria used is 3%/3 mm which was originally recommended by Low *et al*[38]. The user is also capable of setting a lower dose threshold to eliminate dose in the out-of-field region where a large relative dose difference can be calculated and hence skew the γ result[37]. It is customary to report the passing rate (%) of all dose pixels within the evaluated dose distributions. The American Association of Physicists in Medicine Task Group 218 (TG-218) publication highlighted that a stricter gamma criterion of 3%/2 mm is recommended with a 90% pixel passing rate[39].

1.1.4 Current limitations in using the gamma-analysis metric

In recent publications multiple shortcomings have been reported that highlighted the insensitivity of the gamma-analysis metric as a tool for VMAT QA[36,37,40–43]. Most of these articles highlight that while the gamma-analysis method provides a convenient metric for performing VMAT QA, the inherent limitations should be considered before a plan is

approved for treatment. AAPM TG-218 highlighted the spatial resolution of the 2-D array or EPID panel, as well as the interpretation of results as the shortcomings of the gamma analysis metric[44]. The report further emphasized that the review of γ results should not only be limited to the percentage of passing points but should include other relevant γ values such as maximum, mean, minimum and median, as well as a histogram analysis[39].

Despite the issues addressed by TG-218, the gamma-analysis metric also provides no correlation to patient-related clinically useful dose metrics. This was highlighted by Stasi *et al*., who concluded that there is a lack of correlation between gamma-analysis passing rates and Dose-Volume Histogram (DVH) values for Planning Target Volume (PTV) and Organ-at-Risk (OAR) volumes[45,46].

In contrast to older technologies, such as 3D-CRT, current VMAT and IMRT QA protocols explicitly recommend the use of pre-treatment plan verification but make no mention of *in-vivo* dose verification methods. This means that the delivered dose distribution is only verified prior to patient treatment with no verification of the delivered dose to the patient during their multi-fraction radiotherapy course. Hence, the verification of patient dose delivery accuracy relies on the, now proven to be in-sensitive, gamma-analysis metric that is only applied pre-treatment[15,39,47].

Recently, commercial systems became available to use transmission EPID-based dosimetry to verify that the patient's received dose is correct[48–51]. One approach is to use the 3D reconstructed EPID dose to calculate dose-volume histogram (DVH) statistics in the planning computed tomography (pCT) dataset, which in itself does not represent the true dose delivery to the patient[49]. Other commercial approaches allow users to compare first-fraction EPID transmission images to those of all subsequent fractions by means of applying the usual gamma-analysis metric. Although these are useful metrics to quantify the repeatability of treatment fractions, these methods do not provide DVH-specific statistics that relate the delivered dose to the planning target volume (PTV)[48,49,51–54].

Due to the limitations of the gamma-analysis metric, and the retrospective calculation approach used by commercially available systems, several groups have proposed the use of new VMAT QA metrics based on the analysis of dose gradients in 2-D array and EPID images[55,56].

1.1.5 Gradient Dose Segmented Analysis (GDSA) as a proposed new metric for VMAT QA

The gradient dose segmented analysis (GDSA) algorithm was developed by Steers *et al*. to correlate the QA results to clinically relevant endpoints[55,57]. This method allows the use of high-dose low-gradient points to predict changes in the mean PTV dose to quickly evaluate a VMAT QA comparison result. This not only gives more meaningful results in relation to the actual patient dose distribution, but also is a potentially more sensitive metric than the gamma comparison.

This method takes as an input from the user the dose per fraction for a given case, the calculated 2-D dose matrix, and the acquired measurement. The 2-D gradient map at the plane of the detectors is calculated from the 2-D dose map and normalized by the dose per fraction. Thereafter, the locally normalized dose difference maps are created between the calculated and measured doses. Dose differences are segmented into regions of high-gradient and low-gradient. Dose differences in low-gradient regions are further segmented into regions of low-and high-dose based on set thresholds. If the calculated dose is equal to or greater than the threshold, the dose difference at that detector location is labelled as “high-dose low-gradient”, otherwise this will be labelled as “low-dose low-gradient”[55,57].

The GDSA finally calculates the mean of the locally normalized dose differences from all the high-dose low-gradient points and reports this as predicted change in the mean PTV dose between the calculated and measured plan[55,57].

In addition to being employed as a pre-treatment VMAT QA metric, the GDSA can also be used to calculate the change in PTV mean dose over the course of a patient’s multi-

fraction VMAT treatment. The transmission fluence is measured by the EPID during each fraction of the patient's VMAT treatment. If the treatment consists of one or more VMAT arcs, a composite image is obtained by summing the fluence maps (Figure 1-10).

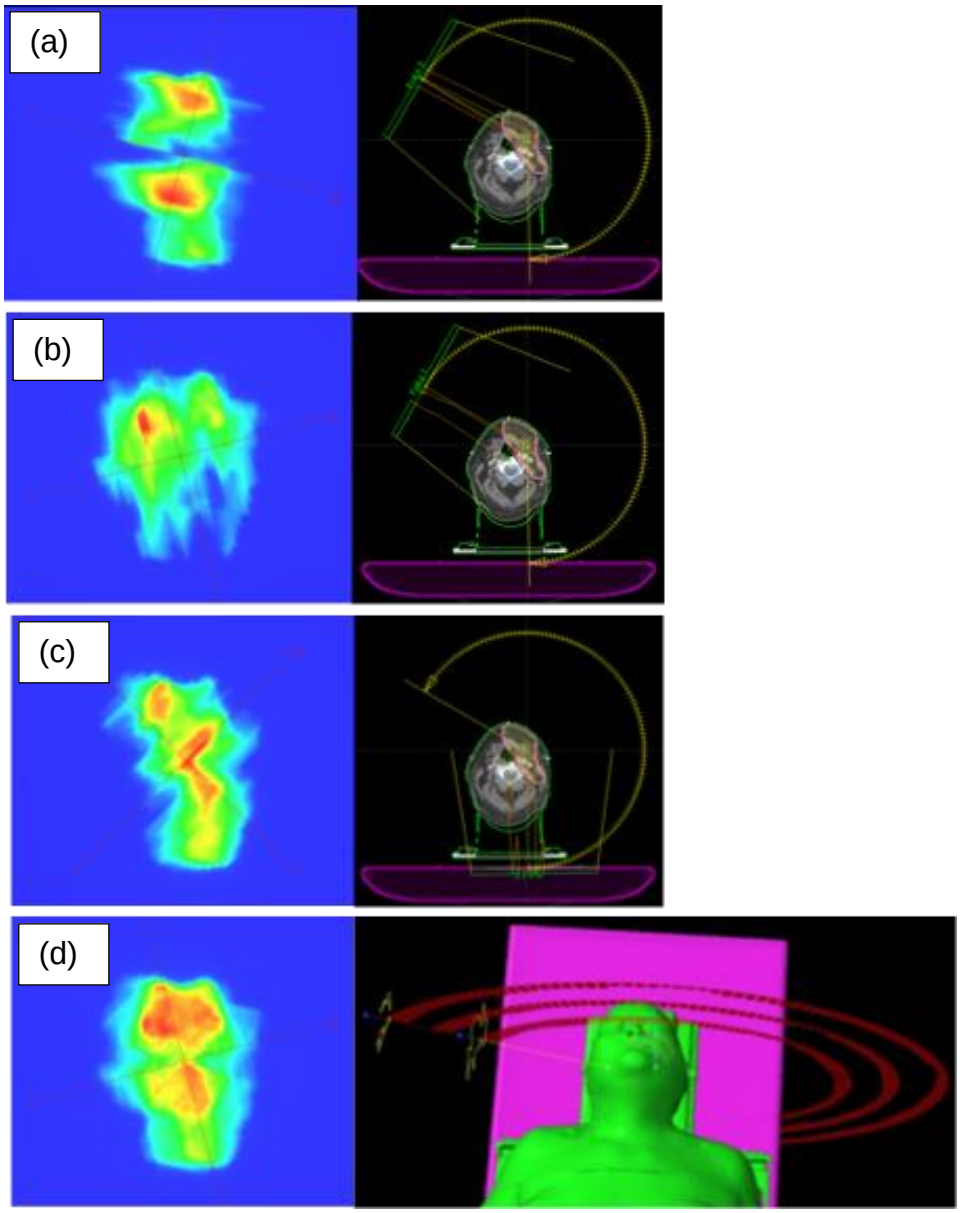

Figure 1-10. The obtained EPID transmission images for (a) – (c) each treatment arc geometry, and (d) the composite image thereof for a VMAT treatment plan.

The composite obtained during the first fraction of treatment is set as the reference fraction. For every subsequent fraction of the treatment, the EPID measured transmission fluence is compared to the reference fraction using the GDSA analysis. This will report the change in PTV mean dose for each treatment fraction.

1.2 Problem Statement

The aim of this project is two-fold: First, it is to apply the GDSA mean metric to detect changes in the mean PTV dose for EBRT patients treated with VMAT; secondly, to identify the causative events for changes in mean PTV dose.

1.3 Central Research Theme and Objectives

The central research theme is establishing a means to evaluate the mean dose delivered to tumour volumes and to identify causative events that would lead to changes in mean PTV dose of patients receiving VMAT treatments for head-and-neck cancers.

The two main objectives are:
Can the GDSA become a useful predictor of treatment delivery quality *in-vivo*?
Can the GDSA be clinically implemented in a resource-constrained environment?

1.4 Research Methodology

Place of research: Radiation Oncology Division, Tygerberg Hospital
Study design: Cohort study
Selection of participants: All 115 patients receiving VMAT external beam radiotherapy treatment for head-and-neck cancers from August 2019 to July 2020.
Exclusion criteria: None.
Methodology: Retrospective analysis of EPID transmission dosimetry images.
Data analysis: The GDSA metric was applied to the EPID transmission images to determine changes in mean PTV dose over the full treatment course. The daily CBCT images were used to calculate changes in anterior-posterior and lateral patient separations for patients with significant changes in PTV mean dose. Additionally, if no separation change was observed, the CBCT images were used to calculate the pitch-,

roll-, and yaw-rotational errors. The maximum and average change in PTV mean dose, rotational errors and separations are reported for the patient group.

2. Chapter 2 – Submitted manuscript: The application of Gradient dose segmented analysis (GDSA) as a treatment quality indicator for patients undergoing Volumetric Modulated Arc Radiotherapy (VMAT)

Journal: Medical Physics
Manuscript reference: 22-1336
Status: Under review (26/08/2022)

Full Title:

The application of gradient dose segmented analysis of in-vivo EPID images for patients undergoing VMAT in a resource-constrained environment.

Short Title:

EPID images as a measure of treatment QA

Authors:

Christoffel Jacobus van Reenen (Corresponding Author; email: ricus@sun.ac.za)
Medical Physics Division, Department of Medical Imaging and Radiation Oncology, Stellenbosch University, Cape Town, WC, South Africa.

Christoph Jan Trauernicht
Medical Physics Division, Department of Medical Imaging and Radiation Oncology, Stellenbosch University, Cape Town, WC, South Africa.

Casey Bojechko
Department of Radiation Medicine and Applied Sciences, University of California San Diego, La Jolla, CA 92037, United States of America.

ABSTRACT

Background:

The gamma analysis metric is a commonly used metric for volumetric modulated arc radiotherapy (VMAT) plan evaluation. The major drawback of this metric is the lack of correlation between gamma passing rates and dose-volume histogram (DVH) values for planning target volumes (PTV). The novel gradient dose segmented analysis (GDSA) metric was developed by *Steers et al*. to quantify changes in the PTV mean dose (D_{mean}) for patients undergoing VMAT.

Purpose:

To apply the GDSA retrospectively to analyze the head-and-neck cancer patients treated on the newly acquired Varian Halcyon in our department, in order to assess changes in PTV D_{mean}, and to evaluate the cause of day-to-day changes in the time-plot series.

Methods:

In-vivo electronic portal imaging device (EPID) transmission images of head-and-neck cancer patients treated between August 2019 and July 2020 on the Varian Halcyon were analyzed retrospectively. The GDSA-predicted changes in PTV D_{mean} were determined for each of the patients treated within the first year of implementation (n = 115 patients). The changes in patient anatomy and rotational positioning errors were quantified using the daily cone-beam computed tomography (CBCT) images and added to a time-plot with the daily change in PTV D_{mean}.

Results:

The GDSA indicated that over 97% of the delivered treatment fractions deviated by less than 3% when compared to the first treatment fraction. 13 of the patients received at least one treatment fraction where the PTV D_{mean} exceeded the 3% threshold. Most of these deviations occurred for the later fractions of radiotherapy treatment. Additionally, 92% of these patients were treated for malignancies involving the larynx and oropharynx with associated long treatment fields. Notable deviations in the effective separation diameters

(defined by the outline of the body contours) were observed for 8 out the 13 patients (62%) where the change in PTV D_{mean} was larger than 3%. In cases where the change in PTV D_{mean} was less than 3%, no notable changes in the effective separation diameters (Δd_{eff}< 3 mm) were observed. For the other 5 cases with GDSA deviations larger than 3%, the pitch, roll and yaw rotational errors were quantified as the Halcyon treatment couch does not allow for rotational corrections. The mean and standard deviation of errors was 0.90º ± 0.89º, 0.45º ± 0.51º and 0.43º ± 0.40º, for pitch, roll, and yaw, respectively.

Conclusions:

The results indicated that large deviations in PTV D_{mean} (>3%) were more likely due to change in separation, whereas small deviations in PTV D_{mean} (<3%) were more likely caused by rotational errors. Weight loss during radiotherapy is well documented and proven to be the highest among head-and-neck cancer patients. Pitch rotational errors were shown to be the most dominant and the reported maximum and mean rotational errors are similar to those reported in literature. The GDSA can easily be implemented to aid the department in scheduling new CT scans for patients experiencing continuous weight loss and setup inaccuracies, before significant deviations in dose delivery occur.

1. INTRODUCTION

The World Health Organization estimates that approximately 70% of deaths from cancer occur in low-and middle-income countries.[1] In South Africa (an upper middle-income country[2]), approximately 107 467 new cancer cases were reported in 2018 alone, along with 57 373 cancer deaths.[3] Roughly 61% of these patients undergo external beam radiation therapy as part of their treatment regime.[4] Radiotherapy departments should have quality assurance (QA) programs in place, to ultimately ensure a high accuracy of treatment dose delivery for all patients.

In addition to patient setup verification, electronic portal imaging devices (EPIDs) have been in routine use to perform various quality control (QC) procedures in radiotherapy. These include multi-leaf collimator (MLC) tests and offline, pre-treatment patient-specific QC procedures for volumetric modulated arc radiotherapy (VMAT) and intensity modulated radiotherapy (IMRT) treatments.[5–7] A variety of EPID-based pre-treatment verification methods have been described in literature; the acquisition can be classified as either non-transmission pre-treatment dosimetry, non-transmission treatment dosimetry, or transmission treatment dosimetry.[6] In addition to the various modes of acquisition, the delivered dose can be estimated using several different approaches, including predicted forward-projected EPID comparisons and simple back-projection of measured data.[6,8–10]

It is becoming increasingly popular to use transmission EPID-based dosimetry to verify that the patient's received dose is correct and multiple commercial systems are now available for use.[6,8,11,12] One such approach is to use the 3D reconstructed EPID dose to calculate dose-volume histogram (DVH) statistics in the planning computed tomography (pCT) dataset. The calculation also approximates all tissues to water, which in itself does not represent the true dose delivery to the patient.[8] Other commercial approaches allow users to compare first-fraction EPID transmission images to those of all subsequent fractions by means of applying the usual gamma-analysis metric. Although these are useful metrics to quantify the repeatability of treatment fractions, these methods do not

provide DVH-specific statistics that relate the delivered dose to the planning target volume (PTV). [6,8,9,12–14]

To address this issue, a new analysis technique was introduced as a pre-treatment verification method in a doctoral dissertation that did not require recalculation of EPID-based data to patient dose, or analysis by means of the pass/fail gamma criteria.[15] Recently, *Steers et al.*[16] published their work on applying the gradient dose segmented analysis (GDSA) technique to in-vivo EPID images for dose verification. Their results showed that the GDSA could successfully predict changes in the PTV mean dose (D_{mean}), a clinically relevant dosimetric endpoint.[16]

The aim of this work is to apply the GDSA analysis method described by *Steers et al* to determine the change in PTV D_{mean} for head-and-neck cancer patients treated with VMAT, and to identify changes in treatment where the GDSA exceeds a 3% threshold. This data was used to determine the treatment quality following the implementation of VMAT for one year and will serve as a baseline for subsequent review.

2. MATERIALS AND METHODS

2.A. Retrospective EPID image data collection

All the EPID images used in this study were acquired on a Varian Halcyon v2.0 linear accelerator, which comes equipped with a 43 cm x 43 cm aS1200 megavoltage imaging panel (Varian Medical Systems, Palo Alto, CA). The panel is mounted directly opposite the single 6 MV flattening filter-free (FFF) beam at a source-to-imager distance (SID) of 154 cm, which corresponds to a 28 cm x 28 cm projection at 100 cm source-axis distance (SAD). The EPID continuously integrates the obtained signal from the entire treatment field during arc treatments. The individually acquired transit images are then automatically exported on an arc-by-arc basis to the record-and-verify system (ARIA, Varian Medical Systems, Palo Alto, CA). The EPID calibration workflow follows a semi-automated step-by-step approach, where dark field and flood field corrections are applied. Thereafter, the EPID is calibrated in terms of Calibrated Units (CU), where 1 CU is equivalent to 1 MU

for a standard 10 cm x 10 cm field size. The linear accelerator's output is verified prior to starting the EPID calibration workflow by following the IAEA TRS-398 code of practice. In addition to monthly output checks, the quality assurance includes the weekly delivery of standard field sequences in QA mode to check the constancy of the EPID response. The Halcyon is also equipped with an automated machine performance check (MPC) which verifies the daily machine output and its drift, along with other parameters.

Approval was granted by the institutional Health Research Ethics Committee (HREC) for the study to proceed. The EPID images were obtained for all head-and-neck cancer radiotherapy patients treated between August 2019 and July 2020. This marked the first year of the simultaneous introduction of the Varian Halcyon, as well as VMAT treatments in our Radiation Oncology Division.

2.B. Retrospective kV CBCT image data collection

In addition to the MV imaging capabilities, the Halcyon is also equipped with a kilovoltage cone-beam computed tomography (kV CBCT) imaging system. All patients treated with VMAT were set up by matching the daily kV CBCT images to pCT images for all treatment fractions. After the acquisition of the daily setup image, the system performs an automated on-line matching between the kV CBCT setup image and the pCT. A team of qualified and trained radiotherapists then verify the image matching and the appropriate couch corrections are applied before treatment. The kV CBCT image and matching with the pCT is automatically exported to the record-and-verify system (ARIA, Varian Medical Systems, Palo Alto, CA) after treatment. The kV CBCT images and registration matrices were obtained for all the head-and-neck cancer radiotherapy patients treated within the study period.

2.C. EPID image analysis using the GDSA algorithm

The collected EPID images were analyzed in MATLAB R2019a (The MathWorks, Inc., Natick, MA) using the GDSA method formulated by *Steers et al*.[15,16] In summary, the

GDSA method takes the acquired EPID reference composite image set for the first treatment fraction as an input and uses the subsequent treatment fraction composite images as the comparison data sets. The dose gradient map is computed using the normalized composite of the reference EPID images. The dose differences between the reference and comparison composite datasets are then calculated and normalized to the dose maximum in the reference dataset. The dose distributions are then segmented into different regions of interest, based on a set dose threshold of 5% and a dose-gradient threshold of 3% relative to the reference data set. This relationship is described by *Moran et al*.[17] in equation (1):

$$G_i = \sqrt{\sum \left(\frac{\Delta d_{ij}}{\Delta x_{ij}}\right)^2} \qquad (1)$$

where G_i is the generalized gradient at a given pixel, i, Δd_{ij} is the dose difference between the pixel i and its four nearest neighbours, j, and Δx_{ij} is the distance between i and j.

For the Varian Halcyon, $\Delta x_{ij} \approx 0.336$ mm, which corresponds to the EPID pixel spacing based on the physical dimensions of the imager panel (43 cm x 43 cm) and image matrix size (1280 x 1280 pixels). The mean percent dose difference in the high-dose, low-gradient regions of the composite distributions has been shown to be a predictor for changes in the PTV D_{mean}. This normalized mean dose difference in the high-dose region is referred to as the GDSA mean, abbreviated as $GDSA_{\mu}$ (%).

The standard deviation of the $GDSA_{\mu}$ was calculated for each treatment fraction as the standard deviation of the distribution of pixels in the region of interest, i.e., the high-dose low-gradient region.

2.D. kV CBCT image analysis: Patient separation

After the EPID images were analyzed using the GDSA, the kV CBCT images of patients where the $|\mathrm{GDSA}\mu| \geq 3\%$ were inspected. The anterior-posterior (A-P) and lateral separations were measured as the absolute change in the outline of the body contour

across the treatment isocenter slice of the kV CBCT for all treatment fractions. The separations were reported as the absolute difference between the reference separation and the separation from subsequent fractions for the A-P direction according to equation (2):

$$\Delta d_{A-P}(cm) = \left|(d_{A-P})_{ref} - (d_{A-P})_n\right| \quad (2)$$

where Δd_{A-P} is the calculated change in anterior-posterior separation (in cm), $(d_{A-P})_{ref}$ is the anterior-posterior separation on the treatment isocenter slice of the reference kV CBCT, and $(d_{A-P})_n$ is the anterior-posterior separation on the treatment isocenter slice of the n subsequent kV CBCTs.

Similarly, the absolute difference for the lateral dimensions were calculated according to equation (3) as:

$$\Delta d_{lat}(cm) = \left|(d_{lat})_{ref} - (d_{lat})_n\right| \quad (3)$$

where Δd_{lat} is the calculated change in lateral separation (in cm), $(d_{lat})_{ref}$ is the lateral separation on the treatment isocenter slice of the reference kV CBCT, and $(d_{lat})_n$ is the lateral separation on the treatment isocenter slice of the n subsequent kV CBCTs.

The effective separation change diameter, $\Delta d_{eff}(cm)$, was then computed using equation (4):

$$\Delta d_{eff}(cm) = \sqrt{\Delta d_{lat} \cdot \Delta d_{A-P}} \quad (4)$$

where Δd_{lat} is the lateral separation change (cm) and Δd_{A-P} is the anterior-posterior separation change (cm). [18]

2.E. kV CBCT image analysis: Rotational set-up corrections

The kV CBCT images were then analyzed in the image registration workspace of the record-and-verify system (ARIA, Varian Medical Systems, Palo Alto, CA) and the rotational corrections were computed for the pitch (θ), roll (ζ) and yaw (φ). The analysis was performed because the Halcyon couch does not allow for online rotational corrections during patient set-up.

3. RESULTS

3.A. Retrospective EPID and kV CBCT image data collection

The EPID and kV CBCT images of patients treated between August 2019 and July 2020 were collected for head-and-neck cancer patients treated with VMAT on the Halcyon. This data set consisted of 115 patients that were treated with 2541 treatment fractions. The patients were categorized by treatment site as listed in Table I. The majority of patients were treated for laryngeal and oropharyngeal cancers.

Table I. The EPID data collected for head-and-neck cancer patients categorized by treatment site.

Treatment and Diagnoses sites	Patients (n)
Larynx	29
Oropharynx (p16-)	27
Lip and Oral Cavity	24
Cervical Lymph Nodes & Unknown Primary tumours	7
Nasal Cavity and Sinuses	7
Hypopharynx	5
Nasopharynx	5
Salivary Glands	5
HPV-Mediated (p16+) Oropharyngeal Cancer	2
Lacrimal Gland	1
Nervous System (Misc.)	1
Orbit	1
Thyroid Gland	1

3.B. EPID image analysis using the GDSA algorithm

For the 2541 fractions, the overall mean of the $GDSA_{\mu}$ values was 0.18% ± 0.66%. From Table II, a total of 82 treatment fractions were delivered where the $|GDSA_{\mu}| \geq 3\%$ and the majority of those were for laryngeal cancers (40 fractions). The mean and standard deviation of the $GDSA_{\mu}$ for the treatment sites where at least one patient treatment fraction had a $|GDSA_{\mu}| \geq 3\%$ are listed in Table III. The largest values of the mean of the $GDSA_{\mu}$

were for the nasopharyngeal, oropharyngeal, and laryngeal treatment sites. Most of these deviations occur during the later treatment fractions.

Table II. Number of patients and total number of fractions per treatment site, and the number of fractions where $|\Delta GDSA_{\mu}| \geq 3\%$.

Tumour site	Patients	Fractions, n (% total)	n fractions $\|\Delta GDSA_{\mu}\| \geq 3\%$.
Larynx	29	641 (25.2%)	40
Oropharynx (p16-)	27	597 (23.5%)	26
Lip and Oral Cavity	24	530 (20.9%)	2
Nasal Cavity and Sinuses	7	155 (6.1%)	7
Unknown Primary H&N tumours	7	155 (6.1%)	0
Hypopharynx	5	110 (4.3%)	1
Nasopharynx	5	110 (4.3%)	3
Salivary Glands	5	110 (4.3%)	3
HPV-Mediated (p16+) Oropharyngeal Cancer	2	44 (1.7%)	0
Lacrimal Gland	1	22 (0.9%)	0
Nervous System (Misc.)	1	23 (0.9%)	0
Orbit	1	22 (0.9%)	0
Thyroid Gland	1	22 (0.9%)	0

Table III. The mean and standard deviation of $GDSA_{\mu}$ for the treatment sites that recorded any fraction where the $|GDSA_{\mu}| \geq 3\%$

Tumour site	n fractions $\|GDSA_{\mu}\| \geq 3\%$	Mean $GDSA_{\mu}$ (%)	STD of $GDSA_{\mu}$
Hypopharynx	1	-0.12	0.53
Lip and Oral Cavity	2	-0.02	0.78
Nasopharynx	3	0.45	0.48
Salivary Glands	3	0.13	0.61
Nasal Cavity and Sinuses	7	0.01	0.59
Oropharynx (p16-)	26	0.27	0.70
Larynx	40	0.25	0.72

There are a few general trends that can be identified when plotting the $GDSA_{\mu}$ as a function of fraction number (n). The first representative plot in Fig. 1 is for a nasal cavity cancer patient. This plot shows that there are minor deviations in the $GDSA_{\mu}$ between treatment fractions and it is generally considered to be stable. This is an indication that the tumor dose remains fairly consistent in each fraction, without major patient anatomical changes or daily setup variations.

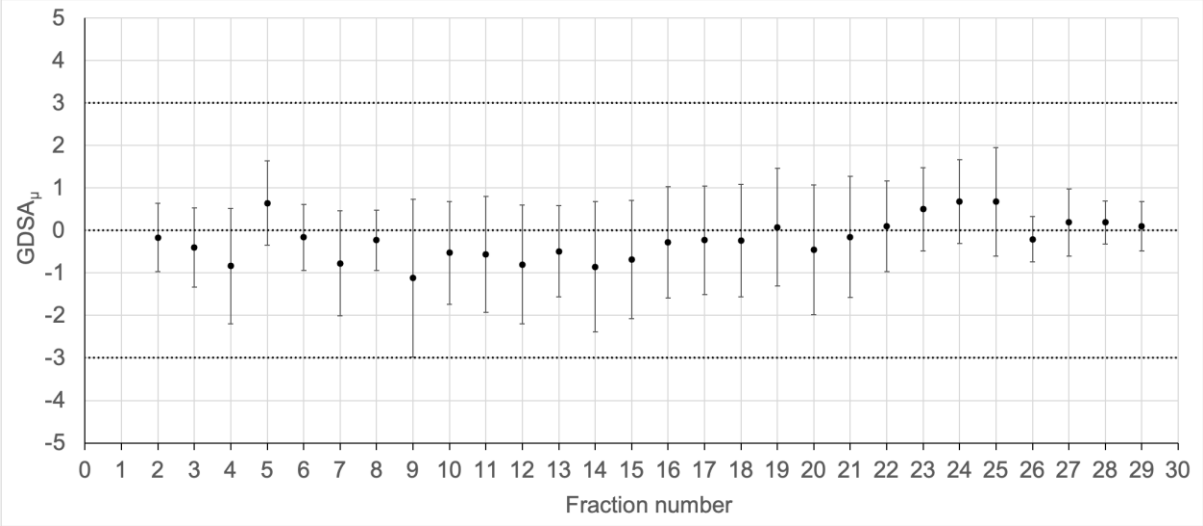

Fig. 1. GDSA$_\mu$ vs fraction number for a nasal cavity cancer patient treated in 29 fractions. Error bars show the standard deviation.

The GDSA$_\mu$ is plotted over 30 fractions for a maxillary sinus patient in Fig. 2. The plot shows a general upwards trend from fraction 25 and is characteristic of the deviations seen in patients where continuous changes in weight and tumor shrinkage occur. In this scenario, the GDSA$_\mu$ does not exceed a 3% threshold; therefore, this patient was not re-planned.

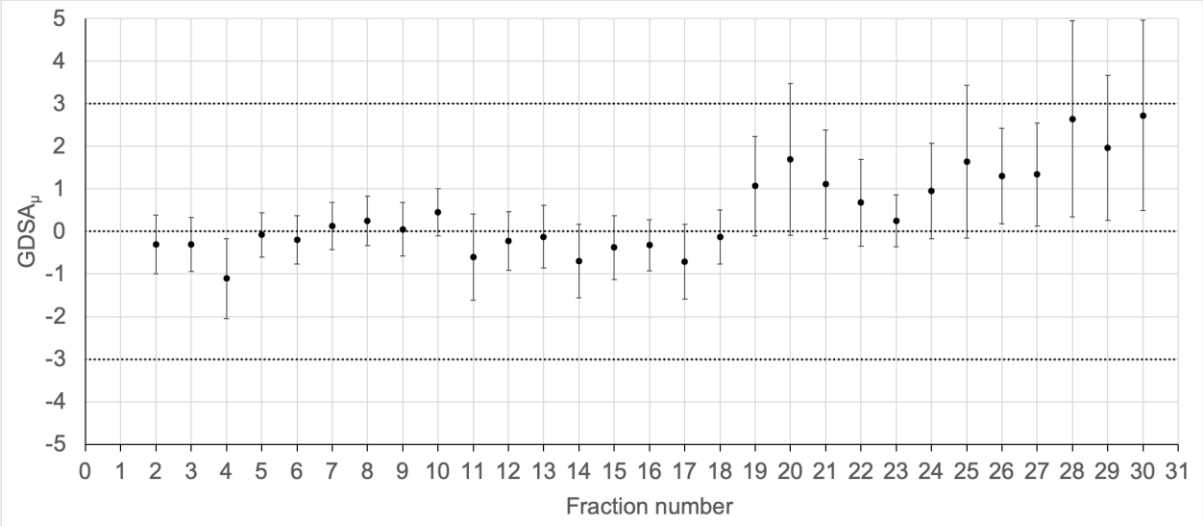

Fig. 2. GDSA$_\mu$ vs fraction number for a maxillary sinus cancer patient treated in 30 fractions. Error bars show the standard deviation.

Fig. 3 represents the plot of $GDSA_{\mu}$ for an oropharyngeal patient treated with 33 fractions. There is a general upwards trend from fraction 21 and the patient could have been replanned before major deviations ($GDSA_{\mu}$ ≥3%) occurred for fractions 24 to 33. If the GDSA had been implemented for daily verification, this could have been flagged on the day, and action could have been taken.

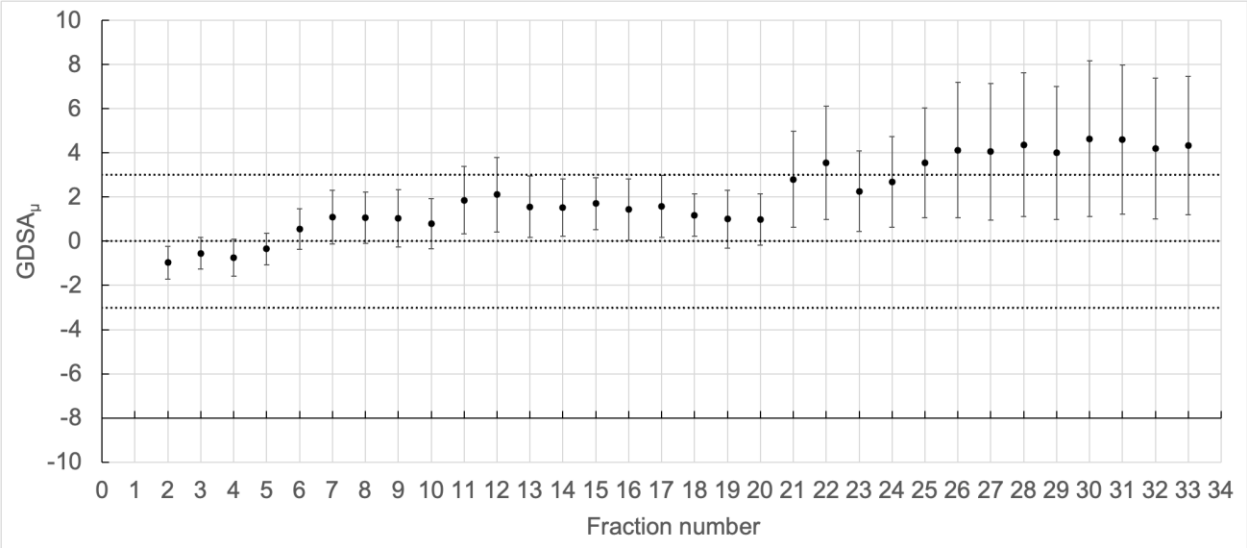

Fig. 3. $GDSA_{\mu}$ vs fraction number for an oropharyngeal cancer patient treated in 33 fractions. Error bars show the standard deviation. Note the number of fractions where $GDSA_{\mu} \geq 3\%$.

The $GDSA_{\mu}$ is plotted over 34 fractions for a nasopharyngeal patient in Fig. 4. The patient was rescanned after fraction 21 and again after fraction 27. There is a gradual upwards trend in $GDSA_{\mu}$ up to fraction 21, which can be attributed to weight loss. Thereafter, the patient was rescanned and replanned, and continued treatment for a further seven fractions. Next, the patient was rescanned again, which pointed to issues radiotherapists had with immobilization and patient positioning during treatment. The patient completed treatment after receiving six more treatment fractions on the new treatment plan.

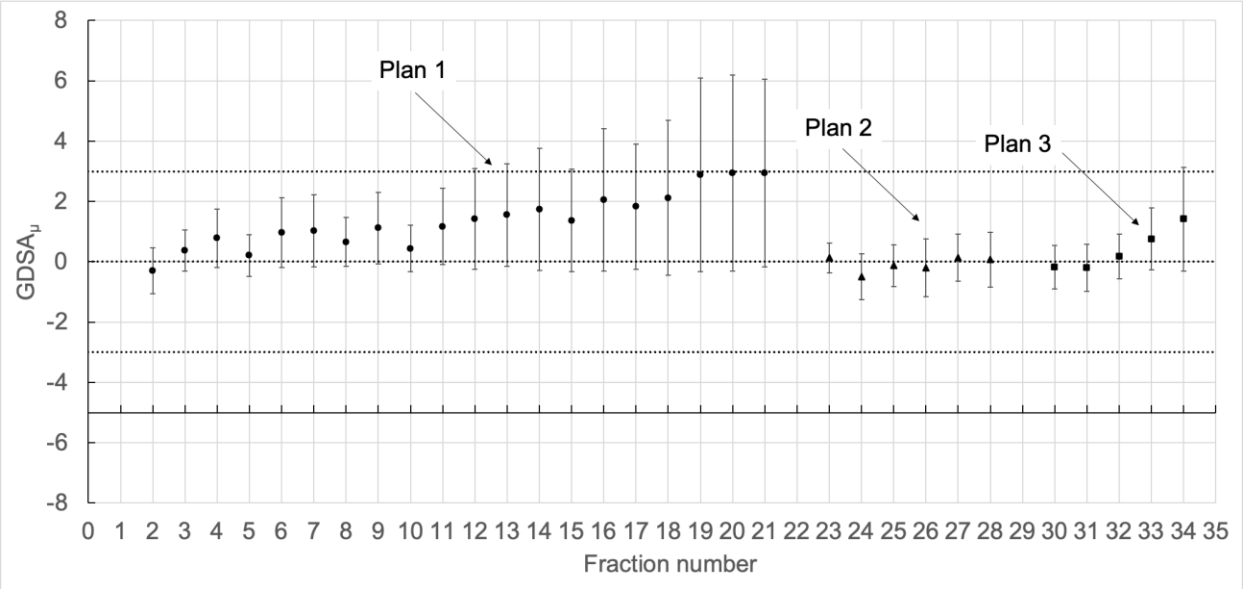

Fig. 4. GDSA$_\mu$ vs fraction number for a nasopharyngeal cancer patient treated in 34 fractions. Error bars show the standard deviation. The first treatment fraction of the new treatment plan was used as reference. Note the number of fractions where GDSA$_\mu$ ≥ 3%.

3.C. kV CBCT image analysis

An in-depth analysis of the kV CBCT images were performed for the thirteen patients where the GDSA$_\mu$ ≥3% for at least one fraction. The maximum measured change in anterior-posterior and lateral separation were $\Delta d_{A-P} = 3.91$ cm and $\Delta d_{Lat} = 3.82$ cm, respectively. The maximum effective separation change diameter was calculated to be $\Delta d_{eff} = 3.86$ cm. In general, Δd_{eff} >1 cm led to a GDSA$_\mu$ ≥3%.

The GDSA$_\mu$ and Δd_{eff} versus the number of fractions for a patient treated over 30 fractions is plotted in Fig. 5. There is a moderate correlation ($R^2 = 0.61$) observed in the plot of the GDSA$_\mu$, versus the effective separation change diameter of the patient during treatment.

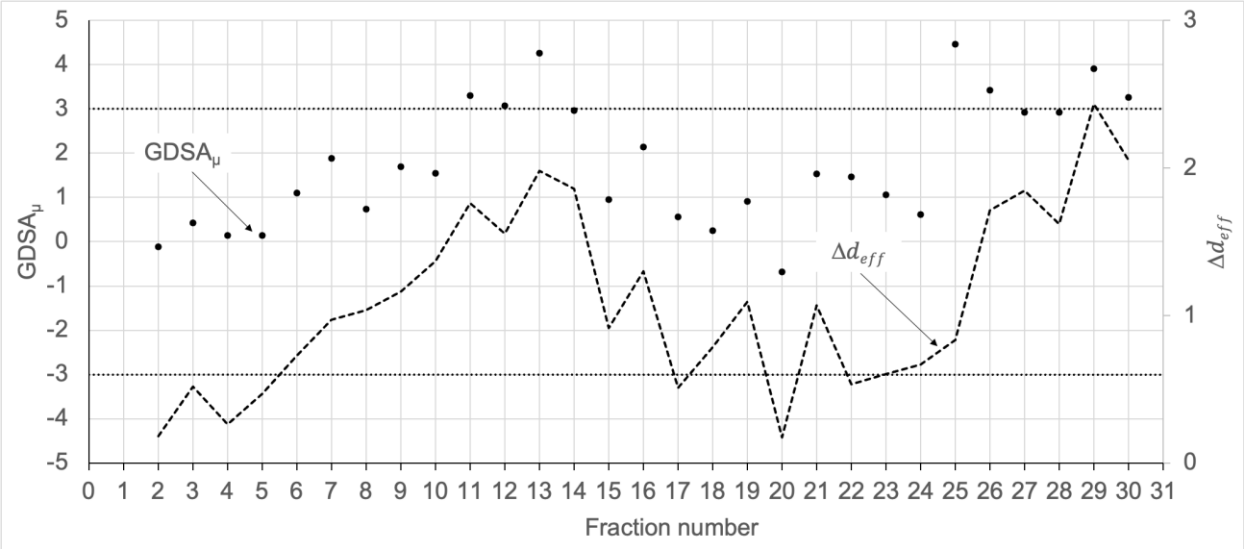

Fig. 5. GDSA$_\mu$ and Δd_{eff} (cm) vs fraction number for a laryngeal cancer patient treated in 30 fractions. Note the number of fractions where GDSA$_\mu$ ≥ 3%.

Fig. 6 is another plot of the GDSA$_\mu$ and Δd_{eff} versus the number of fractions for a patient treated over 30 fractions. A relatively strong correlation was observed (R^2 = 0.82) in this plot. The GDSA$_\mu$ shows a continuous upward trend until the GDSA$_\mu$ ≥3% and the $\Delta d_{eff} >$ 1 cm.

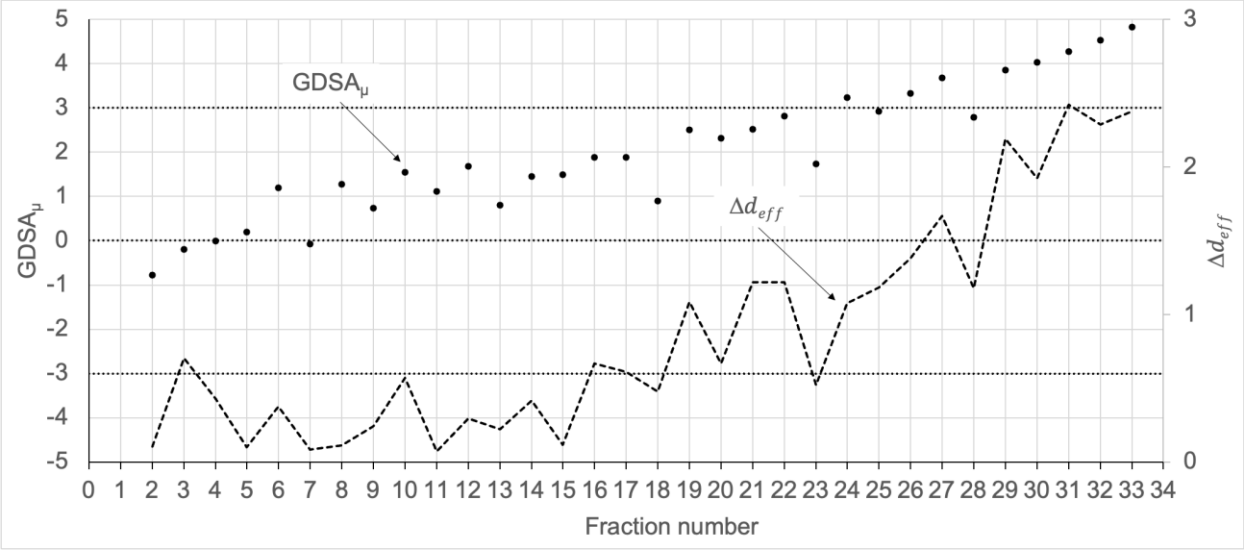

Fig. 6. GDSA$_\mu$ and Δd_{eff} (cm) vs fraction number for an oropharyngeal cancer patient treated in 33 fractions.

The results for the rotational errors of the daily kV CBCT images for the thirteen patients where the $GDSA_{\mu}$ ≥3% for at least one treatment fraction, were calculated and tabulated in Table IV. The maximum rotational errors were calculated as $\theta = 3.90^{o}$, $\zeta = 3.40^{o}$ and $\varphi = 2.59^{o}$, for pitch, roll and yaw, respectively.

Table IV. The maximum, mean and standard deviation of pitch, roll and yaw errors calculated for the thirteen patients where the $|GDSA_{\mu}| \geq 3\%$.

Rotational error	Maximum (degrees)	Mean (degrees)	STD
Pitch	3.90	0.90	0.89
Roll	3.40	0.45	0.51
Yaw	2.60	0.43	0.40

In patients where the $GDSA_{\mu}$ ≥3%, but without changes in separation of $\Delta d_{eff} > 1$ cm, there were errors in pitch between the reference and subsequent fractions. Fig. 7 shows an example plot of the $|GDSA_{\mu}|$ and pitch (θ) versus treatment fractions.

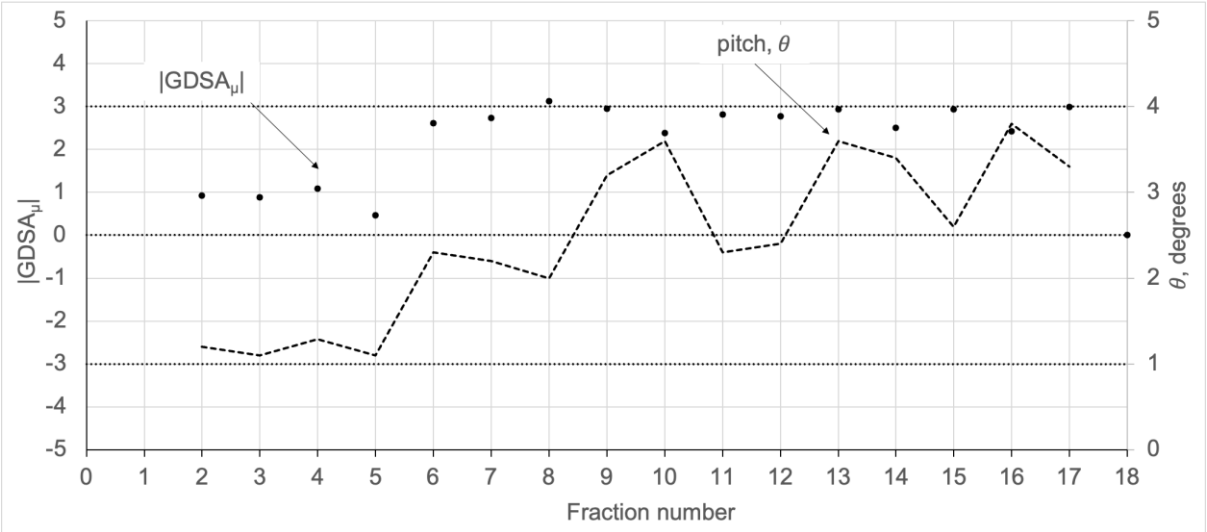

Fig. 7. $|GDSA_{\mu}|$ and pitch (θ, in degrees) vs fraction number for a laryngeal cancer patient treated in 18 fractions.

4. DISCUSSION

The overall mean of the $GDSA_{\mu}$ was 0.18% ± 0.66% which is comparable to the results published by *Steers et al.*[16] for head-and-neck cancer patients treated in their institution. The $GDSA_{\mu}$ exceeded 3% for 82 of 2541 treatment fractions; of these 82, over 48% were patients treated for laryngeal tumors. Plotting the $GDSA_{\mu}$ versus treatment fractions showed a variety of trends that are synonymous with head-and-neck radiotherapy treatments. Firstly, it is showed that many head-and-neck cancer patients continuously lose weight during treatment, and weight-loss causes significant changes in PTV D_{mean} during the later fractions of treatment.

Secondly, it was found that the effective separation change diameter exceeds 1 cm for patients where the $GDSA_{\mu}$ exceeds 3%. *Sun et al.*[19] found that uniform body changes less than 1 cm were unlikely to warrant further assessment due to changes in delivered dose. Similarly, Chen et al.[20] found that the dose delivered to the PTV significantly increased by 2% - 3% for a 2 mm - 5 mm change in body contour. This is an important finding, as it is much easier to implement the $GDSA_{\mu}$ than to measure the effective separation change diameter per fraction for every patient on every treatment day.

For patients were the $|GDSA_{\mu}|$ exceeded 3%, but without an effective separation diameter change of more than 1 cm, significant rotational errors were found. Fig. 7 shows that there is a possible relationship between $|GDSA_{\mu}|$ values and the magnitude of pitch errors in patient setup. The mean and standard deviation in pitch, roll and yaw rotational errors listed in Table IV (0.90º ± 0.89º, 0.45º ± 0.51º and 0.43º ± 0.40º respectively), correspond to the 0.96º ± 1.99º, -0.62º ± 1.44º and -0.17º ± 0.97º found by *Zhang et al.*[21] for head-and-neck patients. Finally, *Guckenberger et al.*[22] showed that rotational errors may be of clinical significance for patients with elongated, non-spherical target volumes and steep dose gradients. Almost half of the $GDSA_{\mu}$ failures in this work were for larynx patients, which tend to be elongated tumors.

5. CONCLUSIONS

The $GDSA_{\mu}$ was able to show clear trends between patient weight changes and changes in the PTV D_{mean}. For patients with minimal weight changes, the pitch was the highest calculated rotational error. However, more data will be needed to fully assess the sensitivity of the $GDSA_{\mu}$ for errors in pitch. The $GDSA_{\mu}$ algorithm is easily implementable and has the means to improve resource allocation in resource-constrained environments. The current data will be used as a baseline in the department's quality assurance program.

6. CONFLICT OF INTEREST

The authors have no relevant conflicts of interest to disclose.

7. REFERENCES

1. World Health Organization. *World Health Statistics 2020*. Vol 1.; 2020.
2. The World Bank Group. World Bank Country and Lending Rates. Published 2020. Accessed March 2, 2021. https://datahelpdesk.worldbank.org/knowledgebase/articles/906519-world-bank-country-and-lending-groups
3. South African National Institute of Communicable Diseases. *National Cancer Registry 2017 Full Report*. Vol 1.; 2020.
4. Barton MB, Frommer M, Shafiq J. Role of radiotherapy in cancer control in low-income and middle-income countries. *Lancet Oncology*. 2006;7(7):584-595. doi:10.1016/S1470-2045(06)70759-8
5. Han B, Ding A, Lu M, Xing L. Pixel response-based EPID dosimetry for patient specific QA. *Journal of Applied Clinical Medical Physics*. 2017;18(1):9-17. doi:10.1002/acm2.12007

6. van Elmpt W, McDermott L, Nijsten S, Wendling M, Lambin P, Mijnheer B. A literature review of electronic portal imaging for radiotherapy dosimetry. *Radiotherapy and Oncology*. 2008;88(3):289-309. doi:10.1016/j.radonc.2008.07.008

7. Grządziel A, Smolińska B, Rutkowski R, Ślosarek K. EPID dosimetry - Configuration and pre-treatment IMRT verification. *Reports of Practical Oncology and Radiotherapy*. 2007;12(6):307-312. doi:10.1016/S1507-1367(10)60069-7

8. Nailon WH, Welsh D, McDonald K, et al. EPID-based in vivo dosimetry using Dosimetry Check™: Overview and clinical experience in a 5-yr study including breast, lung, prostate, and head and neck cancer patients. *Journal of Applied Clinical Medical Physics*. 2019;20(1):6-16. doi:10.1002/acm2.12441

9. Mijnheer B. EPID-based dosimetry and its relation to other 2D and 3D dose measurement techniques in radiation therapy. In: *Journal of Physics: Conference Series*. Vol 847. Institute of Physics Publishing; 2017. doi:10.1088/1742-6596/847/1/012024

10. Wendling M, McDermott LN, Mans A, Sonke JJ, van Herk M, Mijnheer BJ. A simple backprojection algorithm for 3D in vivo EPID dosimetry of IMRT treatments. *Medical Physics*. 2009;36(7):3310-3321. doi:10.1118/1.3148482

11. Feng B, Yu L, Mo E, et al. Evaluation of Daily CT for EPID-Based Transit In Vivo Dosimetry. *Frontiers in Oncology*. 2021;11. doi:10.3389/fonc.2021.782263

12. Fuangrod T, Greer PB, Woodruff HC, et al. Investigation of a real-time EPID-based patient dose monitoring safety system using site-specific control limits. *Radiation Oncology*. 2016;11(1). doi:10.1186/s13014-016-0682-y

13. Bossuyt E, Weytjens R, Nevens D, de Vos S, Verellen D. Evaluation of automated pre-treatment and transit in-vivo dosimetry in radiotherapy using empirically determined parameters. *Physics and Imaging in Radiation Oncology*. 2020;16:113-129. doi:10.1016/j.phro.2020.09.011

14. Ślosarek K, Plaza D, Nas A, et al. Portal dosimetry in radiotherapy repeatability evaluation. *Journal of Applied Clinical Medical Physics*. 2021;22(1):156-164. doi:10.1002/acm2.13123

15. Steers JM. *Quantifying and Improving Error Sensitivity of Intensity Modulated Radiation Therapy Quality Assurance*. 2018.

16. Steers JM, Zavala Bojorquez J, Moore K, Bojechko C. Using in vivo EPID images to detect and quantify patient anatomy changes with gradient dose segmented analysis. *Medical Physics*. 2020;47(11):5419-5427. doi:10.1002/mp.14476

17. Moran JM, Radawski J, Fraass BA. A dose gradient analysis tool for IMRT QA. *Journal of applied clinical medical physics / American College of Medical Physics*. 2005;6(2):62-73. doi:10.1120/jacmp.v6i2.2006

18. Boone J, Strauss K, Cody D, McCollough C, McNitt-Gray M, Toth T. *Size-Specific Dose Estimates (SSDE) in Pediatric and Adult Body CT Examinations*.; 2011.

19. Sun L, Kirkby C, Smith W. Dosimetric effect of body contour changes for prostate and head and neck volumetric modulated arc therapy plans. *Journal of Applied Clinical Medical Physics*. 2019;20(4):115-124. doi:10.1002/acm2.12571

20. Chen C, Fei Z, Chen L, Bai P, Lin X, Pan J. Will weight loss cause significant dosimetric changes of target volumes and organs at risk in nasopharyngeal carcinoma treated with intensity-modulated radiation therapy? *Medical Dosimetry*. 2014;39(1):34-37. doi:10.1016/j.meddos.2013.09.002

21. Zhang L, Garden AS, Lo J, et al. Multiple regions-of-interest analysis of setup uncertainties for head-and-neck cancer radiotherapy. *International Journal of Radiation Oncology Biology Physics*. 2006;64(5):1559-1569. doi:10.1016/j.ijrobp.2005.12.023

22. Guckenberger M, Meyer J, Vordermark D, Baier K, Wilbert J, Flentje M. Magnitude and clinical relevance of translational and rotational patient setup errors: A cone-beam CT study. *International Journal of Radiation Oncology Biology Physics*. 2006;65(3):934-942. doi:10.1016/j.ijrobp.2006.02.019

3. Chapter 3 – Conclusions

3.1 Summary of findings

The $GDSA_{\mu}$ has proven to be sensitive to not only changes in patient anatomy due to weight loss or gain, measurable by determining the effective separation change diameter on kV CBCTs, but has also shown some promise in picking up rotational setup errors for head-and-neck cancer patients treated with long treatment fields.

The mean $GDSA_{\mu}$ was significantly lower than the results reported in the only available publication. While this is a good indication of treatment quality, the published article used a bigger cohort of head-and-neck cancer patients.

In conclusion, the $GDSA_{\mu}$ is easier to implement and less prone to observer bias than calculating the effective change in separation across all treatment fractions for all patients on treatment.

3.2 Future research

Future research will focus on the clinical implementation of the $GDSA_{\mu}$ and the results of the intervention in the Division of Radiation Oncology. Furthermore, the $GDSA_{\mu}$ will be adapted to evaluate dual-isocenter treatment plans for abdomen and pelvis radiotherapy treatments.

4. Chapter 4 – Ethical Considerations

This research project was evaluated by the Health Research Ethics Committee (HREC) of Stellenbosch University via an expedited review process. Ethics exemption was obtained for the initial period 26 March 2021 to 25 March 2022. This was extended for another year to 25 March 2023. See Addendum A and B for exemption letters.

5. Chapter 5 – References

1. Reboux G. Cancer: Key Facts. World Health Organization. doi:10.1007/978-1-137-00443-7_3
2. World Health Organization. *World Health Statistics 2020*. Vol 1.; 2020.
3. South African National Institute of Communicable Diseases. *National Cancer Registry 2017 Full Report*. Vol 1.; 2020.
4. Barton MB, Frommer M, Shafiq J. Role of radiotherapy in cancer control in low-income and middle-income countries. *Lancet Oncology*. 2006;7(7):584-595. doi:10.1016/S1470-2045(06)70759-8
5. Thwaites D. Accuracy required and achievable in radiotherapy dosimetry: Have modern technology and techniques changed our views? *Journal of Physics: Conference Series*. 2013;444(1). doi:10.1088/1742-6596/444/1/012006
6. Kroos J. *An SDE Approach to Cancer Therapy Including Stem Cells*.; 2014. https://www.researchgate.net/publication/293803296
7. Sjogren T. Fall af Epitheliom Behandladt Roentgenstralar. *Forhand Svenska Lakare-Sallsk Sam-mank*. 1899;208.
8. DeVita VT, Rosenberg SA. Two Hundred Years of Cancer Research. *New England Journal of Medicine*. 2012;366(23):2207-2214. doi:10.1056/nejmra1204479
9. Röntgen WC. Ueber eine neue Art von Strahlen. *Ann Phys*. 1898;300(1):12-17. doi:10.1002/andp.18983000103
10. Hajdu SI. A note from history: Landmarks in history of cancer, part 4. *Cancer*. 2012;118(20):4914-4928. doi:10.1002/cncr.27509
11. Taylor L. History of the International Commission on Radiological Protection (ICRP). *Health Phys*. 1958;1(2):97-104.
12. Hajdu SI, Vadmal M. A note from history: Landmarks in history of cancer, Part 6. *Cancer*. 2013;119(23):4058-4082. doi:10.1002/cncr.28319

13. Thwaites DI, Tuohy JB. Back to the future: the history and development of the clinical linear accelerator. *Physics in Medicine and Biology*. 2006;51(13):R343-R362. doi:10.1088/0031-9155/51/13/R20

14. Goitein M, Abrams M, Rowell D, Pollari H, Wiles J. *Multi-Dimensional Treatment Planning: II. Beam's Eye-View, Back Projection, and Projection through CT Sections.* Vol 9.; 1983.

15. Vatnitsky S, Rosenblatt E, International Atomic Energy Agency. *Transition from 2-D Radiotherapy to 3-D Conformal and Intensity Modulated Radiotherapy.* International Atomic Energy Agency; 2008.

16. Brahme A. Optimal setting of multileaf collimators in stationary beam radiation therapy. *Strahlentherapie und Onkologie : Organ der Deutschen Rontgengesellschaft . [et al]*. 1988;164(6):343-350.

17. Boyer A, Biggs P, Galvin J, et al. *Basic Applications of Multileaf Collimators*.; 2001. doi:10.37206/71

18. Webb S. Optimization by simulated annealing of three-dimensional conformal treatment planning for radiation fields defined by a multileaf collimator. *Physics in Medicine and Biology*. 1991;36(9):1201-1226. doi:10.1088/0031-9155/36/9/004

19. Otto K. Volumetric modulated arc therapy: IMRT in a single gantry arc. *Medical Physics*. 2008;35(1):310-317. doi:10.1118/1.2818738

20. Teoh M, Clark CH, Wood K, Whitaker S, Nisbet A. Volumetric modulated arc therapy: A review of current literature and clinical use in practice. *British Journal of Radiology*. 2011;84(1007):967-996. doi:10.1259/bjr/22373346

21. Xing L, Chen Y, Luxton G, Li JG, Boyer AL. Monitor unit calculation for an intensity modulated photon field by a simple scatter-summation algorithm. *Physics in Medicine and Biology*. 2000;45(3). doi:10.1088/0031-9155/45/3/401

22. Elith CA, Dempsey SE, Cao F, Farshadi A, Warren-Forward HM. The quality assurance of volumetric modulated arc therapy (VMAT) plans for early stage

prostate cancer: A technical note. *Journal of Medical Radiation Sciences*. 2014;61(4):261-266. doi:10.1002/jmrs.78

23. Olch AJ. Dosimetric performance of an enhanced dose range radiographic film for intensity-modulated radiation therapy quality assurance. *Medical Physics*. 2002;29(9):2159-2168. doi:10.1118/1.1500398

24. Low DA, Chao KSC, Mutic S, Gerber RL, Perez CA, Purdy JA. Quality assurance of serial tomotherapy for head and neck patient treatments. *International Journal of Radiation Oncology Biology Physics*. 1998;42(3):681-692. doi:10.1016/S0360-3016(98)00273-9

25. Dogan N, Leybovich LB, Sethi A. Comparative evaluation of Kodak EDR2 and XV2 films for verification of intensity modulated radiation therapy. *Physics in Medicine and Biology*. 2002;47(22):4121-4130. doi:10.1088/0031-9155/47/22/314

26. Childress NL, Salehpour M, Dong L, Bloch C, White RA, Rosen II. Dosimetric accuracy of Kodak EDR2 film for IMRT verifications. *Medical Physics*. 2005;32(2):539-548. doi:10.1118/1.1852791

27. Guo PY, Adamovics JA, Oldham M. Characterization of a new radiochromic three-dimensional dosimeter. *Medical Physics*. 2006;33(5):1338-1345. doi:10.1118/1.2192888

28. Jursinic PA, Nelms BE. A 2-D diode array and analysis software for verification of intensity modulated radiation therapy delivery. *Medical Physics*. 2003;30(5):870-879. doi:10.1118/1.1567831

29. Feygelman V, Zhang G, Stevens C, Nelms BE. Evaluation of a new VMAT QA device, or the “X” and “O” array geometries. *Journal of Applied Clinical Medical Physics*. 2011;12(2):146-168. doi:10.1120/jacmp.v12i2.3346

30. Spezi E, Angelini AL, Romani F, Ferri A. Characterization of a 2D ion chamber array for the verification of radiotherapy treatments. *Physics in Medicine and Biology*. 2005;50(14):3361-3373. doi:10.1088/0031-9155/50/14/012

31. Stasi M, Giordanengo S, Cirio R, et al. D-IMRT verification with a 2D pixel ionization chamber: Dosimetric and clinical results in head and neck cancer. *Physics in Medicine and Biology*. 2005;50(19):4681-4699. doi:10.1088/0031-9155/50/19/017

32. Shukaili K Al, Petasecca M, Newall M, et al. A 2D silicon detector array for quality assurance in small field dosimetry: DUO: *Medical Physics*. 2017;44(2):628-636. doi:10.1002/mp.12060

33. Moran JM, Roberts DA, Nurushev TS, Antonuk LE, El-Mohri Y, Fraass BA. An Active Matrix Flat Panel Dosimeter (AMFPD) for in-phantom dosimetric measurements. *Medical Physics*. 2005;32(2):466-472. doi:10.1118/1.1855012

34. Warkentin B, Steciw S, Rathee S, Fallone BG. Dosimetric IMRT verification with a flat-panel EPID. *Medical Physics*. 2003;30(12):3143-3155. doi:10.1118/1.1625440

35. Low DA, Harms WB, Mutic S, Purdy JA. A technique for the quantitative evaluation of dose distributions. *Medical Physics*. 1998;25(5):656-661. doi:10.1118/1.598248

36. Song JH, Kim MJ, Park SH, et al. Gamma analysis dependence on specified low-dose thresholds for VMAT QA. *Journal of Applied Clinical Medical Physics*. 2015;16(6):263-272. doi:10.1120/jacmp.v16i6.5696

37. Hussein M, Clark C, Nisbet A. Challenges in calculation of the gamma index in radiotherapy – Towards good practice. *Physica Medica*. 2017;36:1-11. doi:10.1016/j.ejmp.2017.03.001

38. Low DA, Harms WB, Mutic S, Purdy JA. A technique for the quantitative evaluation of dose distributions. *Medical Physics*. 1998;25(5):656-661. doi:10.1118/1.598248

39. Miften M, Olch A, Mihailidis D, et al. Tolerance limits and methodologies for IMRT measurement-based verification QA: Recommendations of AAPM Task Group No. 218. *Medical Physics*. 2018;45(4):e53-e83. doi:10.1002/mp.12810

40. Nelms B, Jarry G, Chan M, Hampton C, Watanabe Y, Feygelman V. Real-world examples of sensitivity failures of the 3%/3mm pass rate metric and published action levels when used in IMRT/VMAT system commissioning. *Journal of Physics: Conference Series*. 2013;444(1):6-11. doi:10.1088/1742-6596/444/1/012086

41. Oldham M, Sakhalkar H, Guo P, Adamovics J. An investigation of the accuracy of an IMRT dose distribution using two- and three-dimensional dosimetry techniques. *Medical Physics*. 2008;35(5):2072-2080. doi:10.1118/1.2899995

42. Basran PS, Woo MK. An analysis of tolerance levels in IMRT quality assurance procedures. *Medical Physics*. 2008;35(6):2300-2307. doi:10.1118/1.2919075

43. Vieillevigne L, Molinier J, Brun T, Ferrand R. Gamma index comparison of three VMAT QA systems and evaluation of their sensitivity to delivery errors. *Physica Medica*. 2015;31(7):720-725. doi:10.1016/j.ejmp.2015.05.016

44. Miften M, Olch A, Mihailidis D, et al. Tolerance limits and methodologies for IMRT measurement-based verification QA: Recommendations of AAPM Task Group No. 218. *Medical Physics*. 2018;45(4):e53-e83. doi:10.1002/mp.12810

45. Stasi M, Bresciani S, Miranti A, Maggio A, Sapino V, Gabriele P. Pretreatment patient-specific IMRT quality assurance: A correlation study between gamma index and patient clinical dose volume histogram. *Medical Physics*. 2012;39(12):7626-7634. doi:10.1118/1.4767763

46. Nelms BE, Zhen H, Tomé WA. Per-beam, planar IMRT QA passing rates do not predict clinically relevant patient dose errors. *Medical Physics*. 2011;38(2):1037-1044. doi:10.1118/1.3544657

47. Elith CA, Dempsey SE, Cao F, Farshadi A, Warren-Forward HM. The quality assurance of volumetric modulated arc therapy plans for early stage prostate cancer: a technical note. *Journal of Medical Radiation Sciences*. 2014;61(4):261-266. doi:10.1002/jmrs.78

48. van Elmpt W, McDermott L, Nijsten S, Wendling M, Lambin P, Mijnheer B. A literature review of electronic portal imaging for radiotherapy dosimetry. *Radiotherapy and Oncology*. 2008;88(3):289-309. doi:10.1016/j.radonc.2008.07.008

49. Nailon WH, Welsh D, McDonald K, et al. EPID-based in vivo dosimetry using Dosimetry Check™: Overview and clinical experience in a 5-yr study including

breast, lung, prostate, and head and neck cancer patients. *Journal of Applied Clinical Medical Physics*. 2019;20(1):6-16. doi:10.1002/acm2.12441

50. Feng B, Yu L, Mo E, et al. Evaluation of Daily CT for EPID-Based Transit In Vivo Dosimetry. *Frontiers in Oncology*. 2021;11. doi:10.3389/fonc.2021.782263

51. Fuangrod T, Greer PB, Woodruff HC, et al. Investigation of a real-time EPID-based patient dose monitoring safety system using site-specific control limits. *Radiation Oncology*. 2016;11(1). doi:10.1186/s13014-016-0682-y

52. Mijnheer B. EPID-based dosimetry and its relation to other 2D and 3D dose measurement techniques in radiation therapy. In: *Journal of Physics: Conference Series*. Vol 847. Institute of Physics Publishing; 2017. doi:10.1088/1742-6596/847/1/012024

53. Bossuyt E, Weytjens R, Nevens D, de Vos S, Verellen D. Evaluation of automated pre-treatment and transit in-vivo dosimetry in radiotherapy using empirically determined parameters. *Physics and Imaging in Radiation Oncology*. 2020;16:113-129. doi:10.1016/j.phro.2020.09.011

54. Ślosarek K, Plaza D, Nas A, et al. Portal dosimetry in radiotherapy repeatability evaluation. *Journal of Applied Clinical Medical Physics*. 2021;22(1):156-164. doi:10.1002/acm2.13123

55. Steers JM, Zavala Bojorquez J, Moore K, Bojechko C. Using in vivo EPID images to detect and quantify patient anatomy changes with gradient dose segmented analysis. *Medical Physics*. 2020;47(11):5419-5427. doi:10.1002/mp.14476

56. Moran JM, Radawski J, Fraass BA. A dose gradient analysis tool for IMRT QA. *Journal of applied clinical medical physics / American College of Medical Physics*. 2005;6(2):62-73. doi:10.1120/jacmp.v6i2.2006

57. Steers JM. *Quantifying and Improving Error Sensitivity of Intensity Modulated Radiation Therapy Quality Assurance*. 2018.

Addendum A

UNIVERSITEIT STELLENBOSCH UNIVERSITY

Approval Notice

New Application

26/03/2021

Project ID: 21795

HREC Reference No: X21/03/005

Project Title: Application of Gradient Dose Segmented Analysis as a Plan Quality Indicator for Patients Undergoing Volumetric Modulated Arc Radiotherapy

Dear Mr. Christoffel Van Reenen

The **New Application** received on 08/03/2021 13:33 was reviewed by members of **Health Research Ethics Committee** via **expedited** review procedures on 26/03/2021 and was approved.

Please note the following information about your approved research protocol:

Protocol Approval Date: 26 March 2021

Protocol Expiry Date: 25 March 2022

Please remember to use your Project ID 21795 and Ethics Reference Number X21/03/005 on any documents or correspondence with the HREC concerning your research protocol.

Please note that the HREC has the prerogative and authority to ask further questions, seek additional information, require further modifications, or monitor the conduct of your research and the consent process.

After Ethical Review

Translation of the informed consent document(s) to the language(s) applicable to your study participants should now be submitted to the HREC.

Please note you can submit your progress report through the online ethics application process, available at: Links Application Form Direct Link and the application should be submitted to the HREC before the year has expired. Please see *Forms and Instructions* on our HREC website (www.sun.ac.za/healthresearchethics) for guidance on how to submit a progress report.

The HREC will then consider the continuation of the project for a further year (if necessary). Annually a number of projects may be selected randomly for an external audit.

Please note that for studies involving the use of questionnaires, the final copy should be uploaded on Infonetica.

Provincial and City of Cape Town Approval

Please note that for research at a primary or secondary healthcare facility, permission must still be obtained from the relevant authorities (Western Cape Departement of Health and/or City Health) to conduct the research as stated in the protocol. Please consult the Western Cape Government website for access to the online Health Research Approval Process, see: https://www.westerncape.gov.za/general-publication/health-research-approval-process. Research that will be conducted at any tertiary academic institution requires approval from the relevant hospital manager. Ethics approval is required BEFORE approval can be obtained from these health authorities.

We wish you the best as you conduct your research.

For standard HREC forms and instructions, please visit: Forms and Instructions on our HREC website https://applyethics.sun.ac.za/ProjectView/Index/21795

If you have any questions or need further assistance, please contact the HREC office at 021 938 9677.

Yours sincerely,

Mrs. Brightness Nxumalo
HREC 2 Coordinator

National Health Research Ethics Council (NHREC) Registration Number:

REC-130408-012 (HREC1)•REC-230208-010 (HREC2)

Page 1 of 2

Addendum B

Stellenbosch UNIVERSITY IYUNIVESITHI UNIVERSITEIT

forward together
sonke siya phambili
saam vorentoe

Approval Letter
Progress Report

22/02/2022

Project ID: 21795

Ethics Reference No: X21/03/005

Project Title: Application of Gradient Dose Segmented Analysis as a Plan Quality Indicator for Patients Undergoing Volumetric Modulated Arc Radiotherapy

Dear Mr CJ Van Reenen

We refer to your request for an extension/annual renewal of ethics approval dated 05/01/2022.

The Health Research Ethics Committee reviewed and approved the annual progress report through an expedited review process.

The approval of this project is extended for a further year.

Approval date: 26 March 2022

Expiry date: 25 March 2023

Kindly be reminded to submit progress reports two (2) months before expiry date.

Where to submit any documentation

Kindly note that the HREC uses an electronic ethics review management system, *Infonetica*, to manage ethics applications and ethics review process. To submit any documentation to HREC, please click on the following link: https://applyethics.sun.ac.za.

Please remember to use your Project Id 21795 and ethics reference number X21/03/005 on any documents or correspondence with the HREC concerning your research protocol.

Please note that for studies involving the use of questionnaires, the final copy should be uploaded on Infonetica.

Yours sincerely,

Mrs A Fortuin
Health Research Ethics Committee 2 (HREC2)

National Health Research Ethics Council (NHREC) Registration Number:
REC-130408-012 (HREC1)•REC-230208-010 (HREC2)

Federal Wide Assurance Number: 00001372
Office of Human Research Protections (OHRP) Institutional Review Board (IRB) Number:
IRB0005240 (HREC1)•IRB0005239 (HREC2)

The Health Research Ethics Committee (HREC) complies with the SA National Health Act No. 61 of 2003 as it pertains to health research. The HREC abides by the ethical norms and principles for research, established by the World Medical Association (2013), Declaration of Helsinki: Ethical Principles for Medical Research Involving Human Subjects; the South African Department of Health (2006).Guidelines for Good Practice in the Conduct of Clinical Trials with Human Participants in South Africa (2nd edition); as well as the Department of Health (2015). Ethics in Health Research: Principles, Processes and Structures (2nd edition).

The Health Research Ethics Committee reviews research involving human subjects conducted or supported by the Department of Health and Human Services, or other federal departments or agencies that apply the Federal Policy for the Protection of Human Subjects to such research (United States Code of Federal Regulations Title 45 Part 46); and/or clinical investigations regulated by the Food and Drug Administration (FDA) of the Department of Health and Human Services.

Page 1 of 1

Addendum C – GDSA plots for all patients*

*Plots for all treatment plans consisting of more than 3 treatment fractions.

*Multiple plots may exist for patients with more than one treatment plan.

C1 – Cervical Lymph Nodes & Unknown Primary tumours

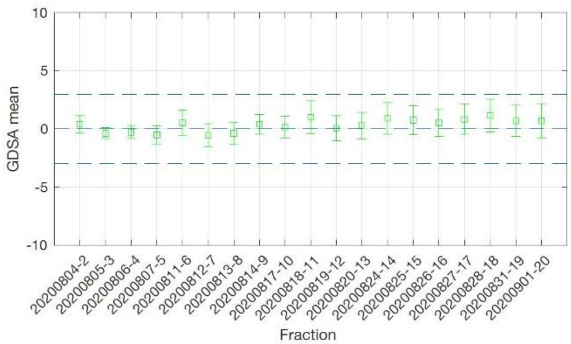

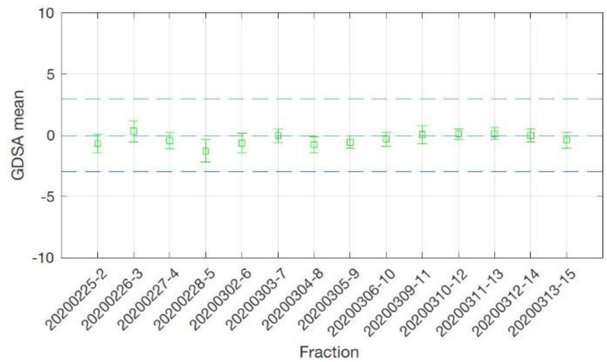

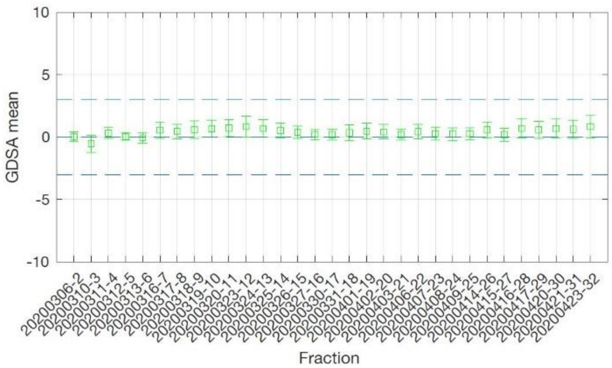

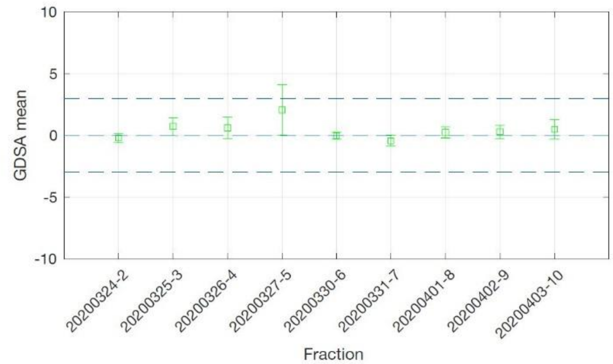

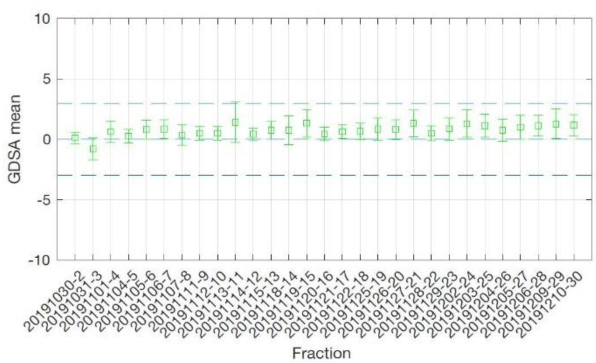

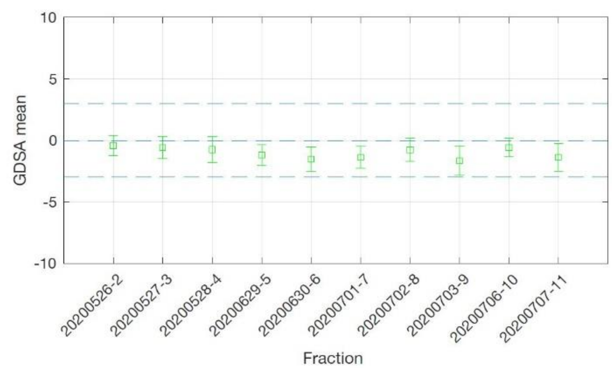

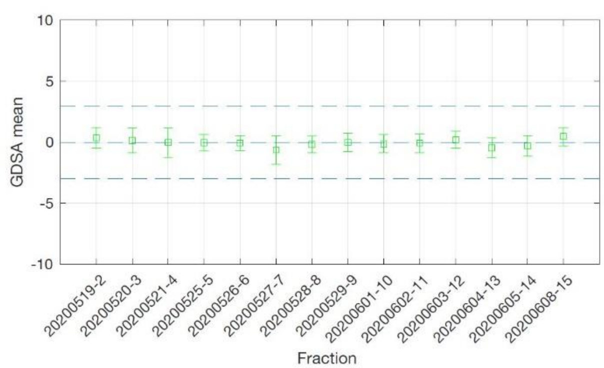

C2 – HPV-Mediated (p16+) Oropharyngeal Cancer

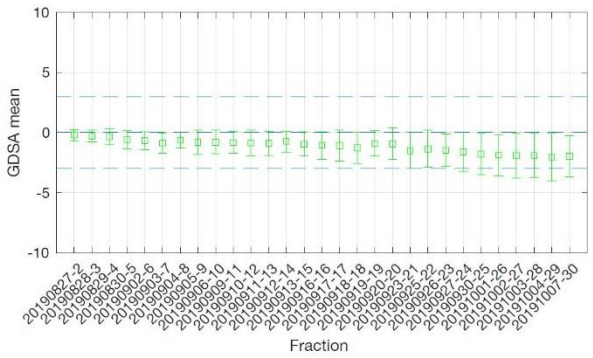

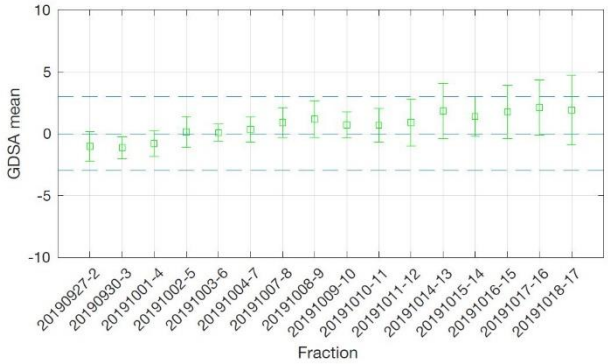

C3 – Hypopharyngeal Cancer

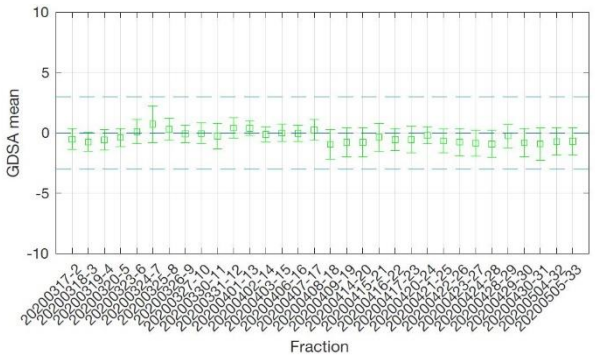

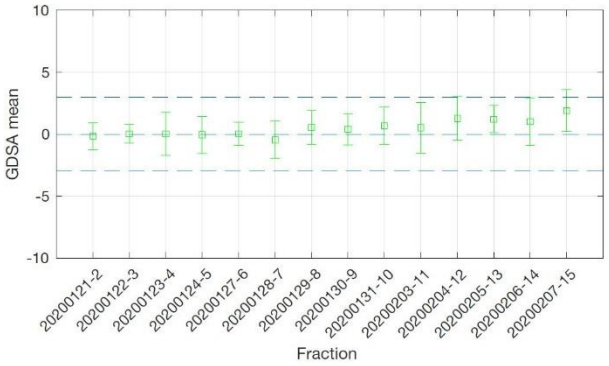

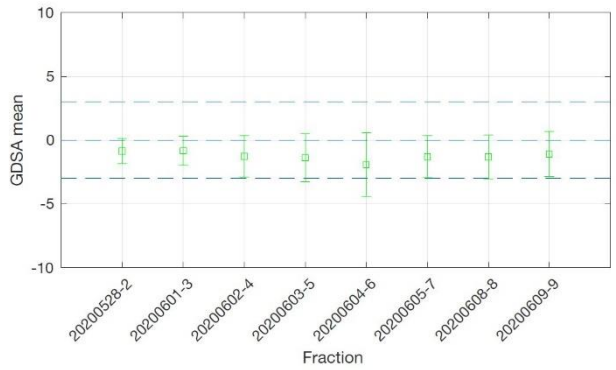

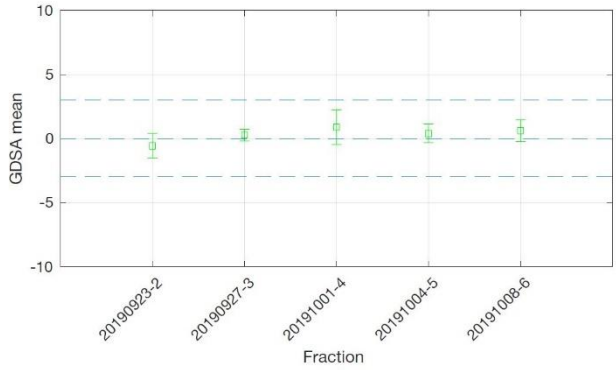

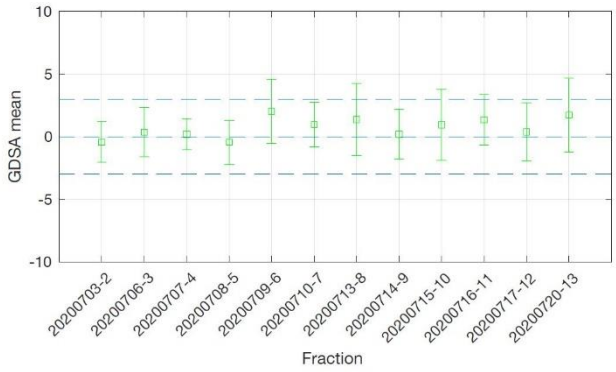

C4 – Lacrimal gland Cancers

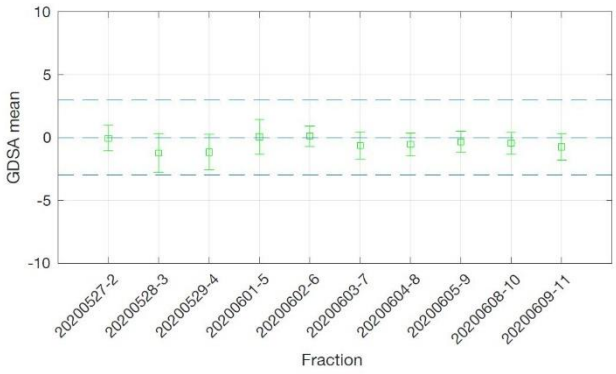

C5 – Laryngeal Cancers

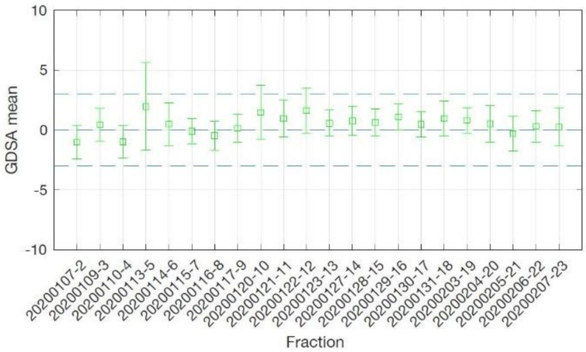

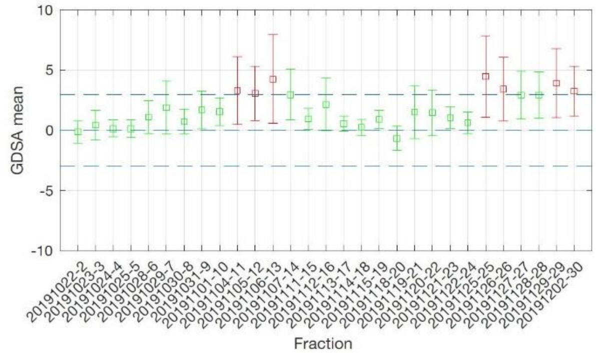

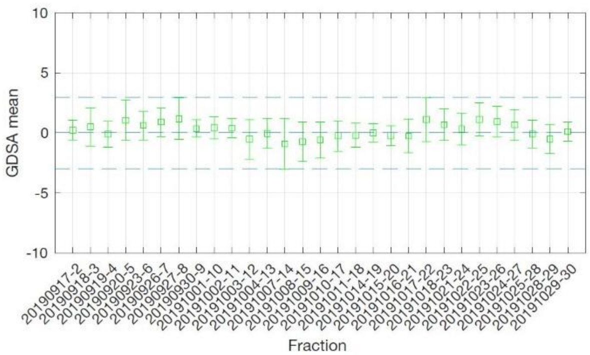

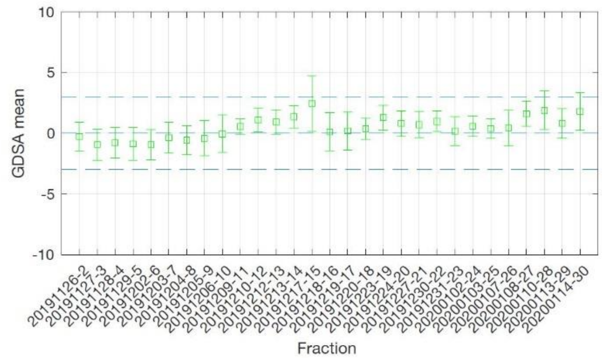

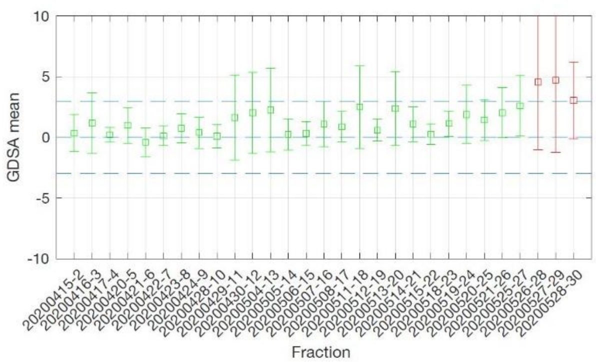

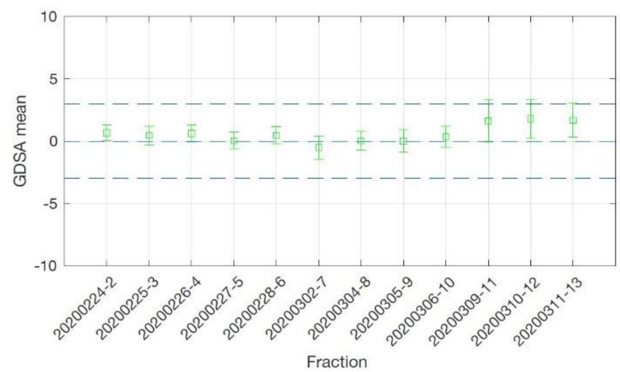

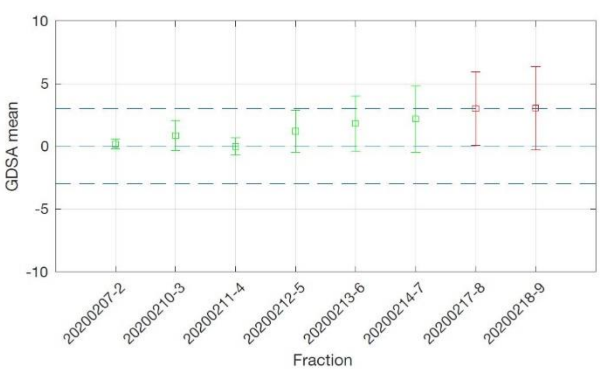

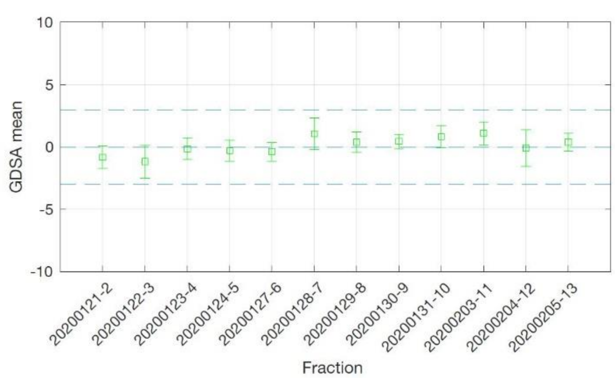

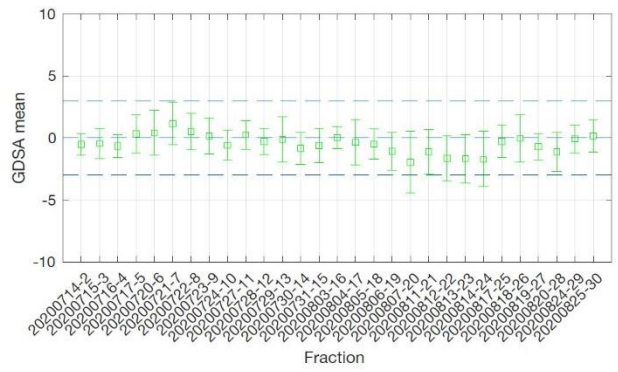

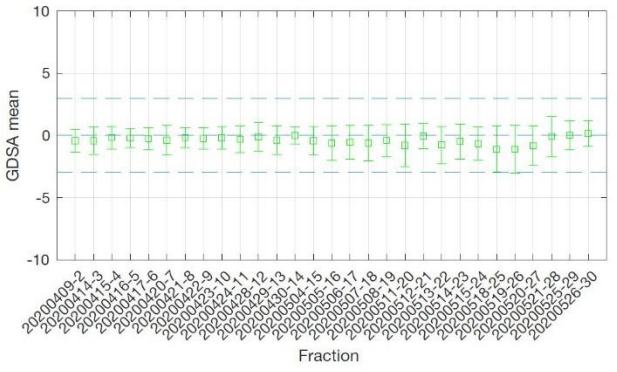

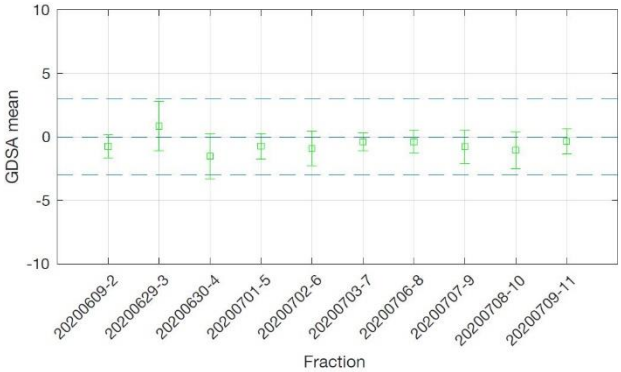

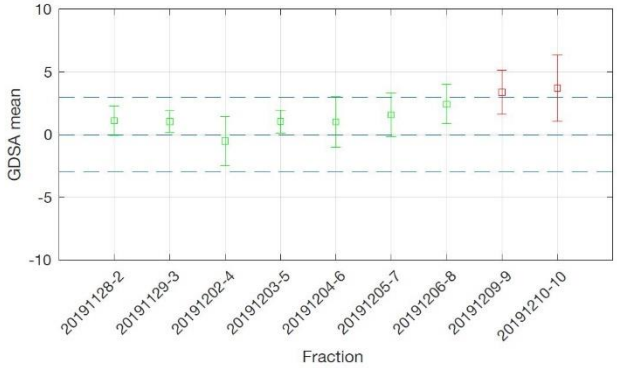

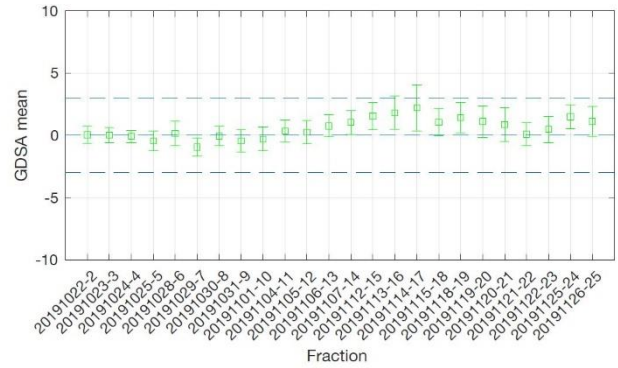

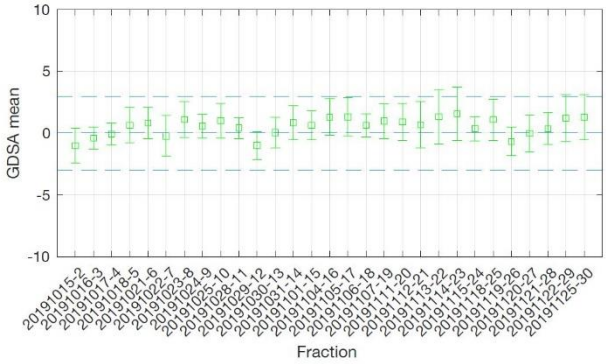

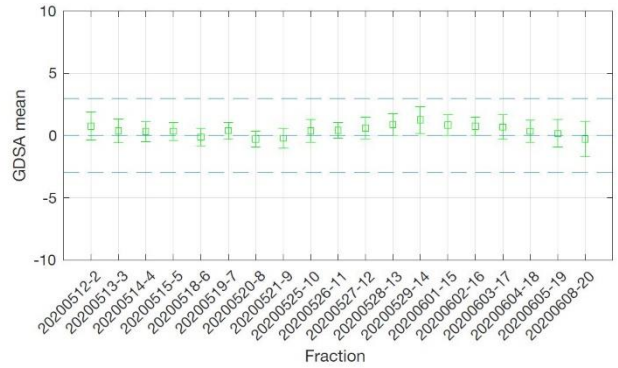

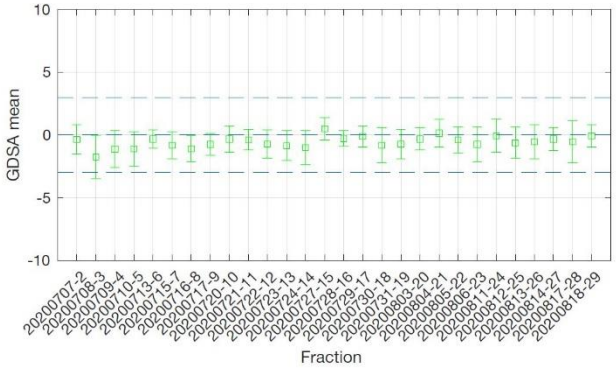

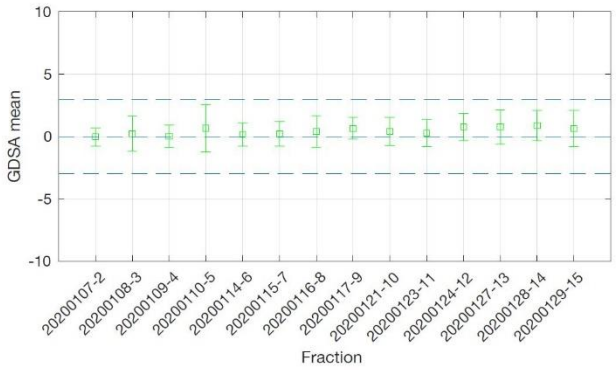

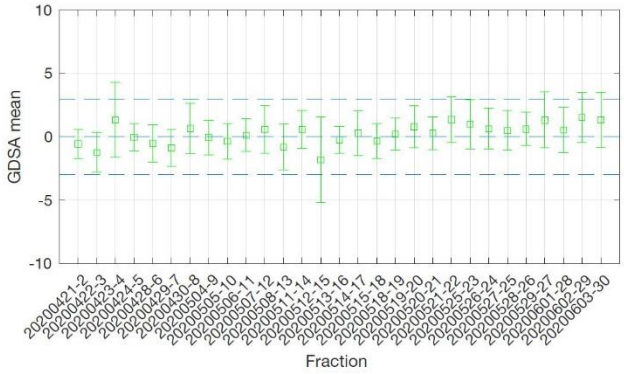

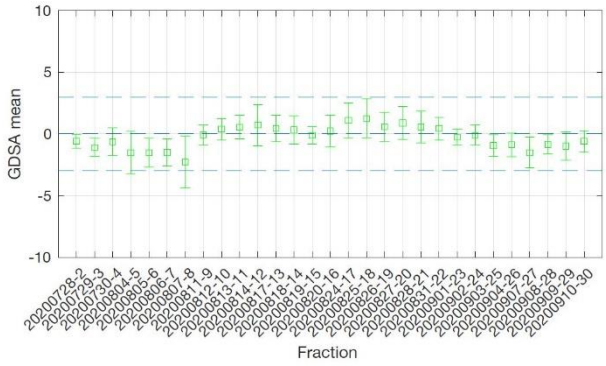

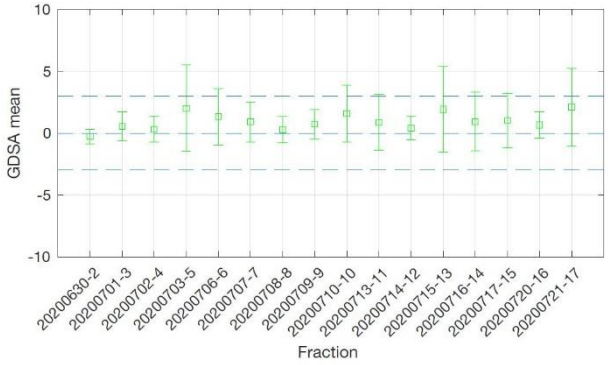

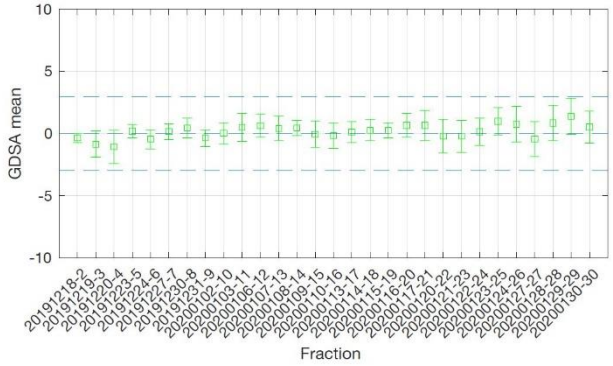

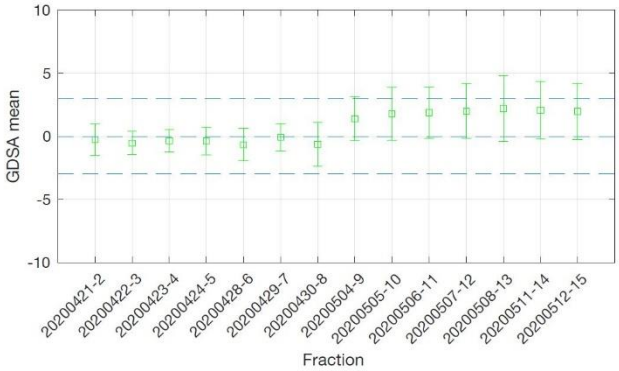

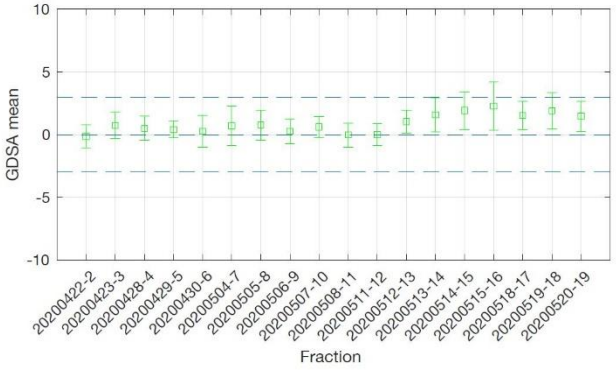

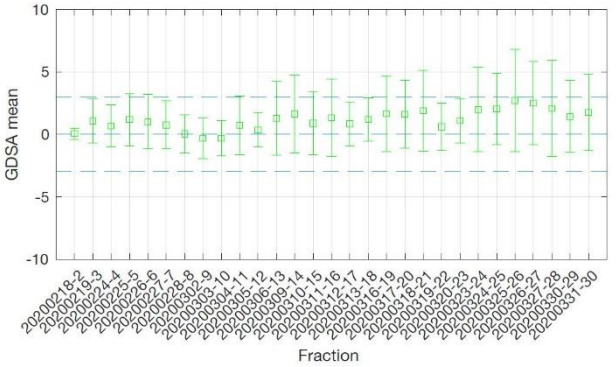

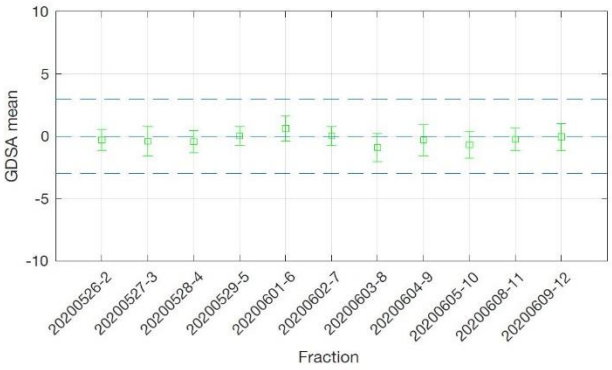

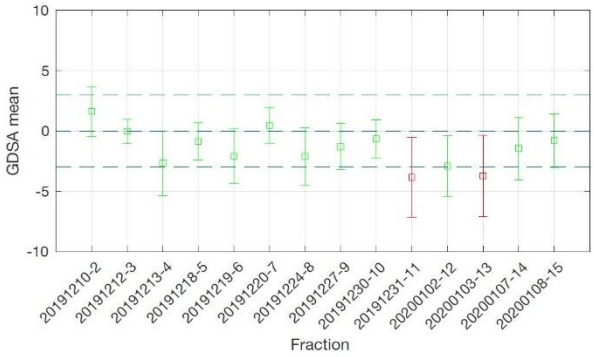

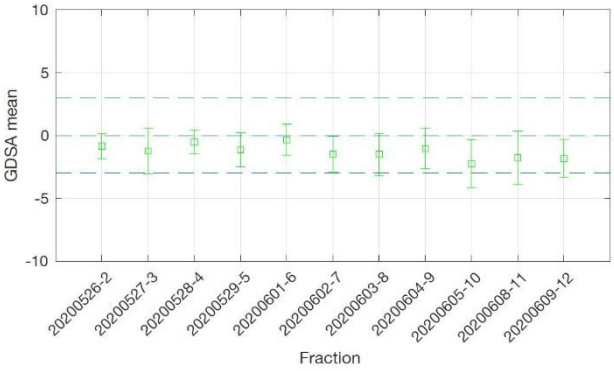

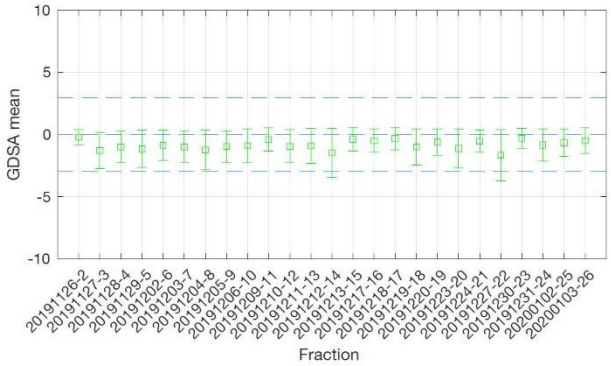

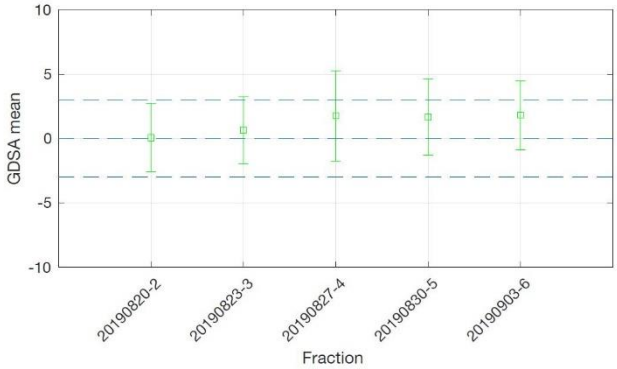

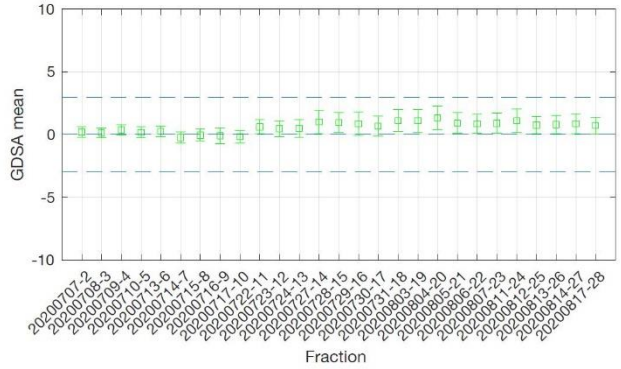

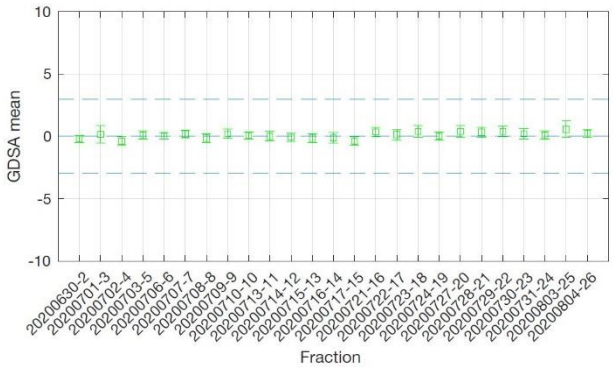

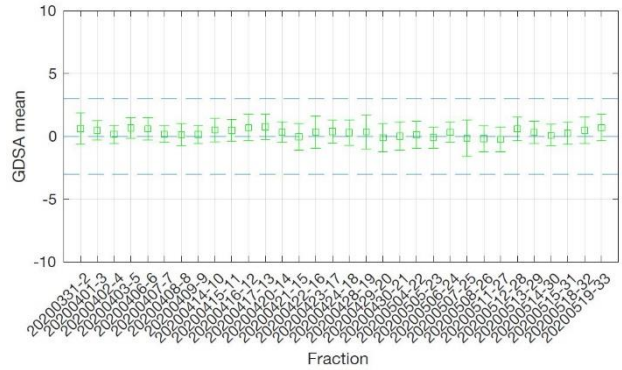

C6 – Lip and Oral Cavity cancers

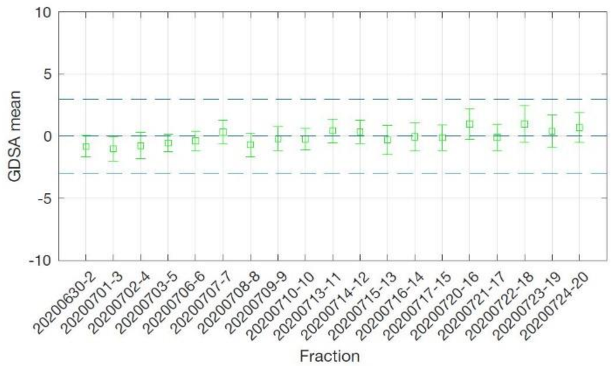

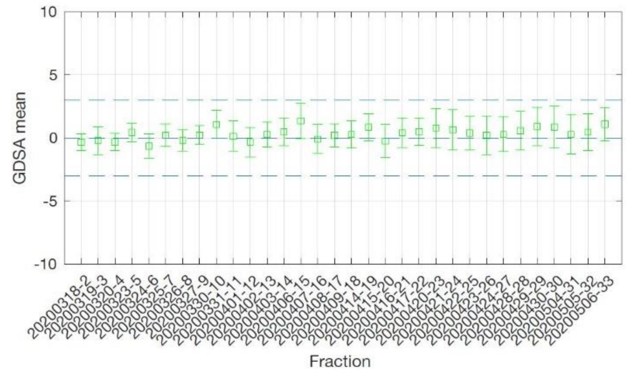

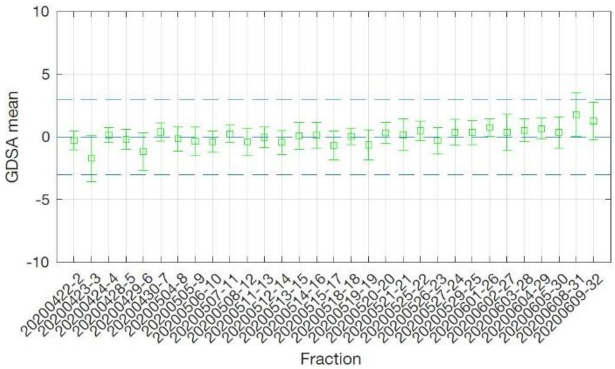

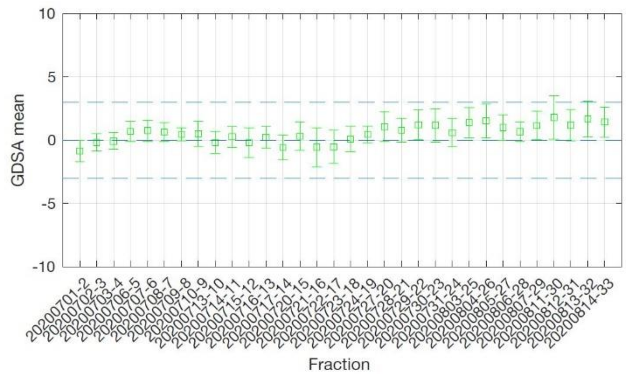

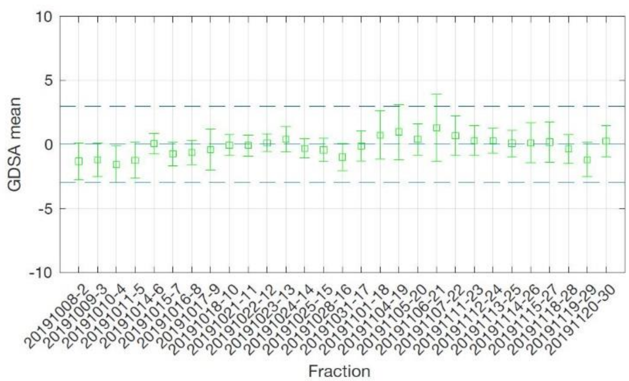

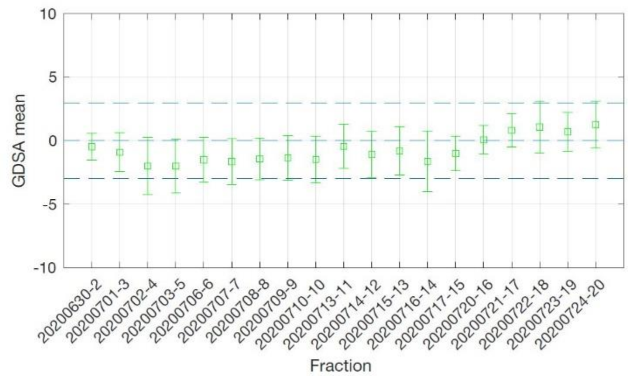

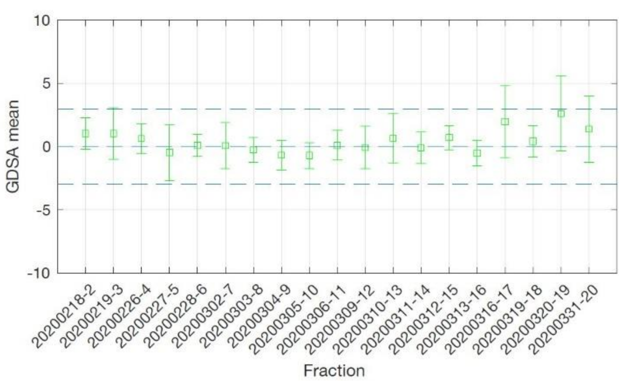

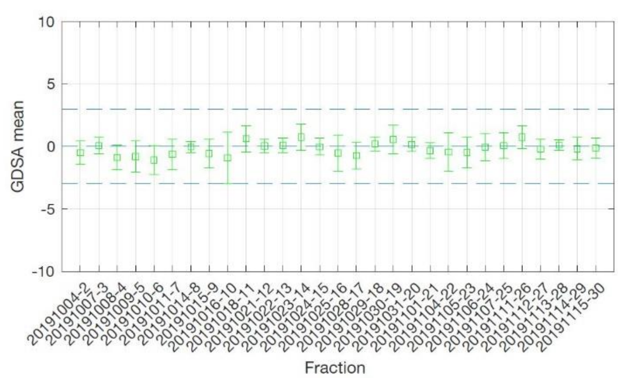

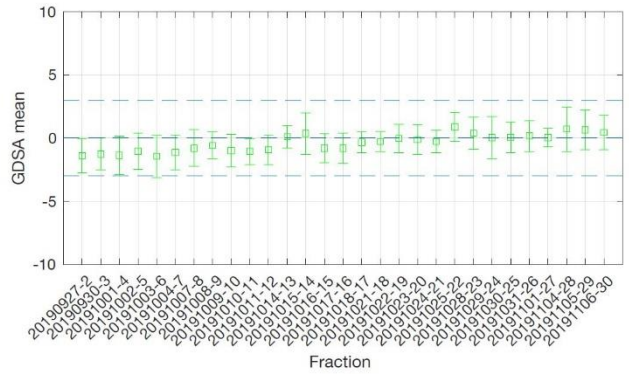

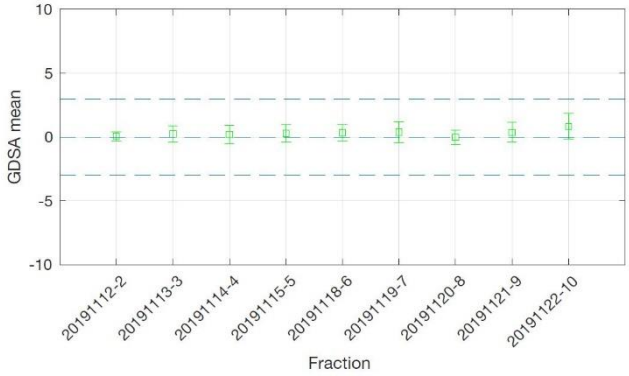

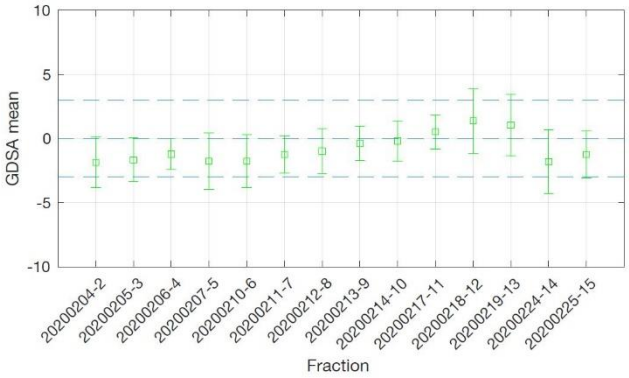

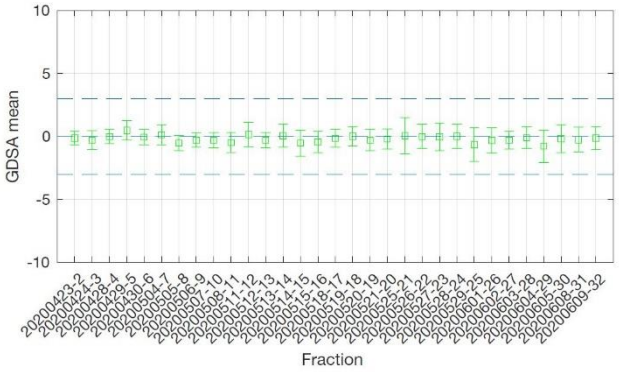

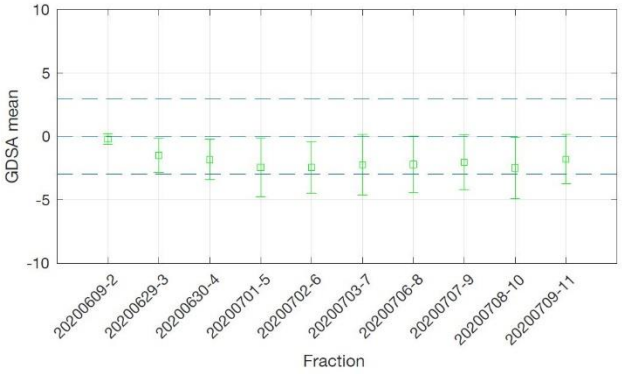

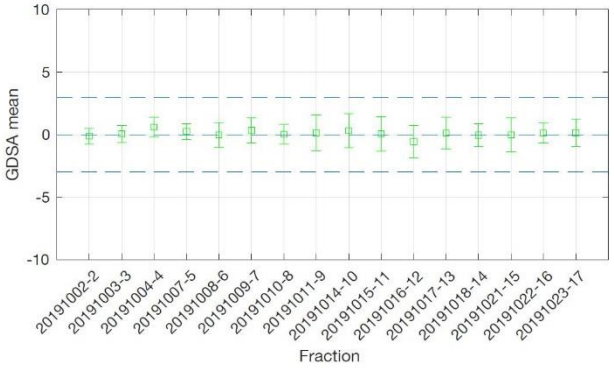

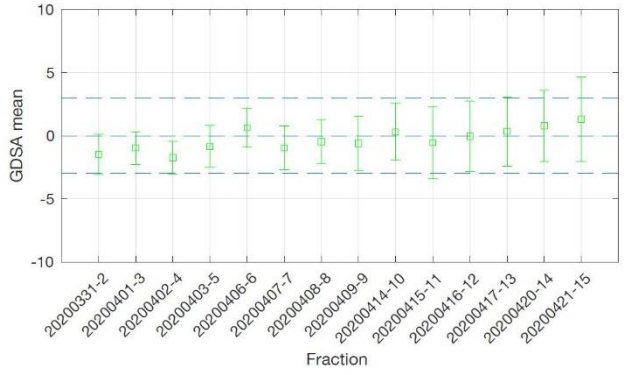

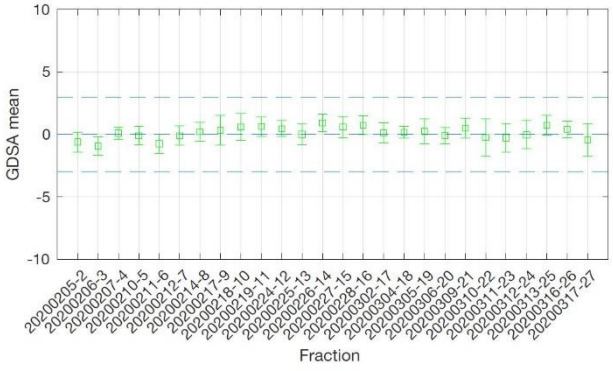

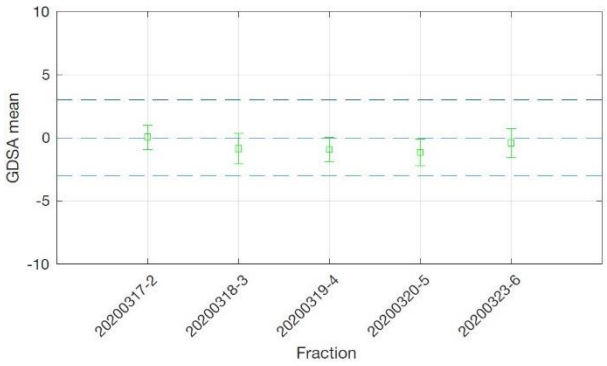

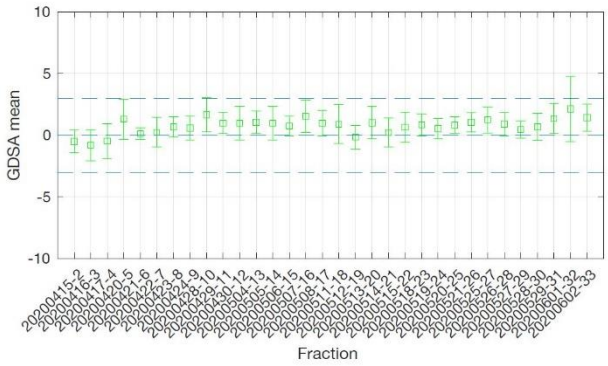

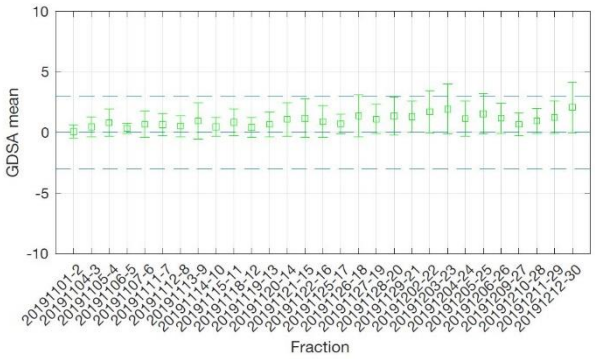

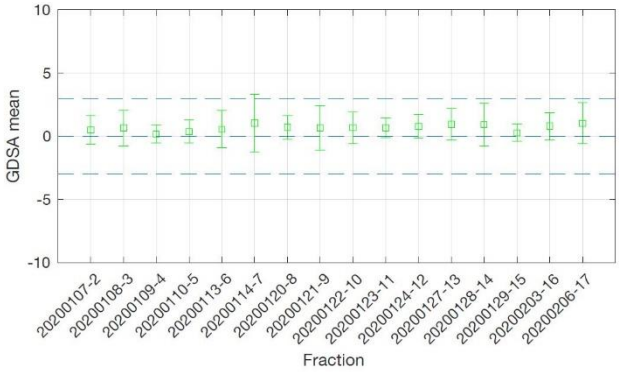

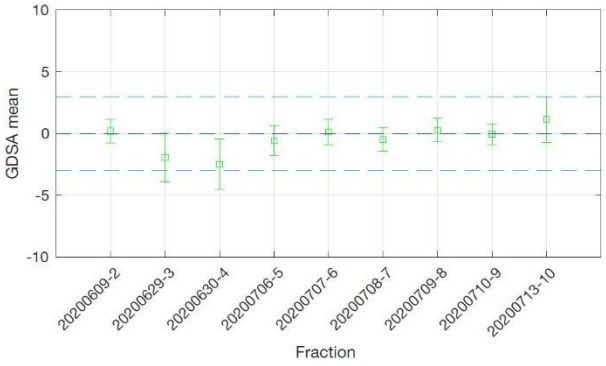

C7 – Nasal Cavity and Sinuses cancers

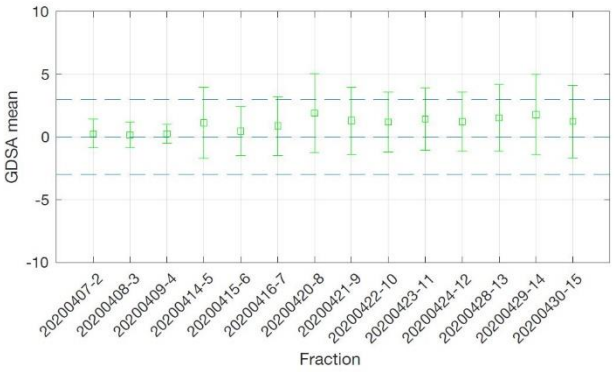

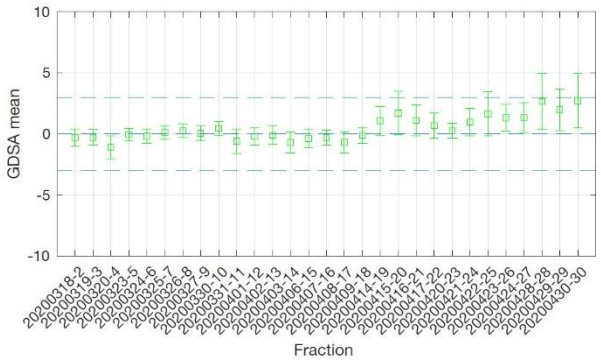

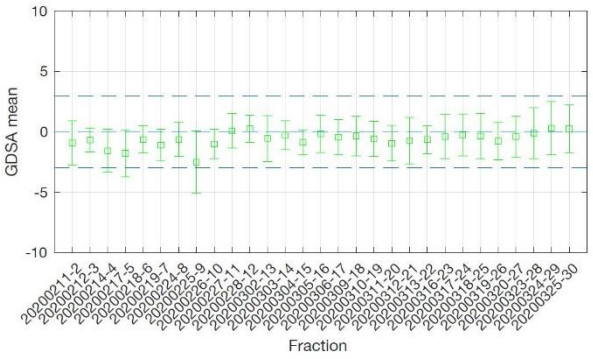

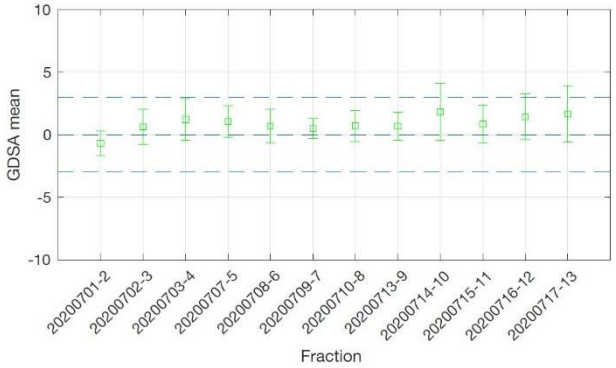

C8 – Nasopharyngeal cancers

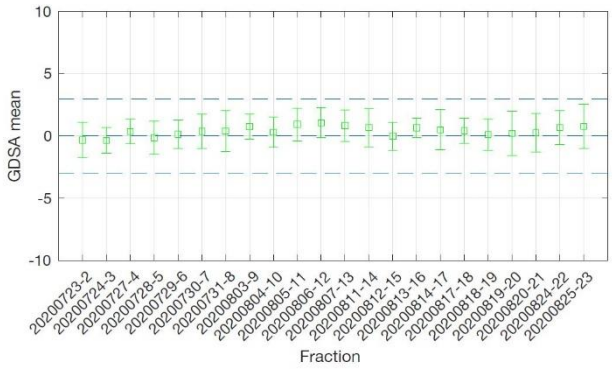

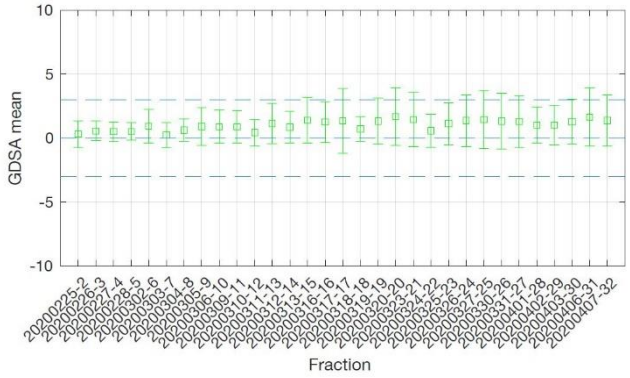

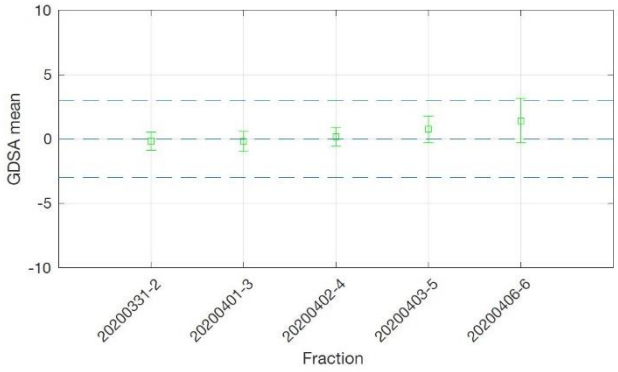

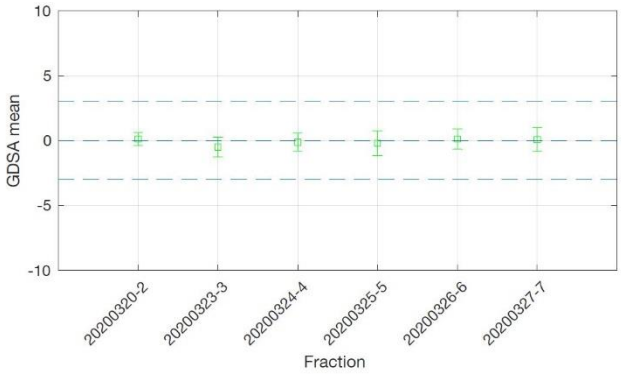

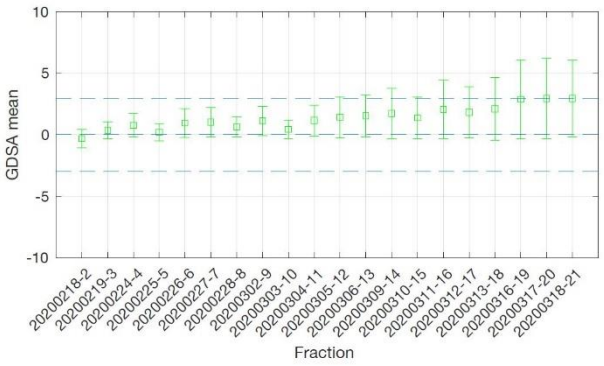

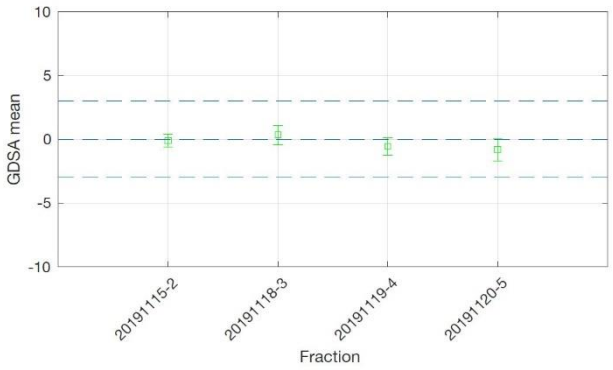

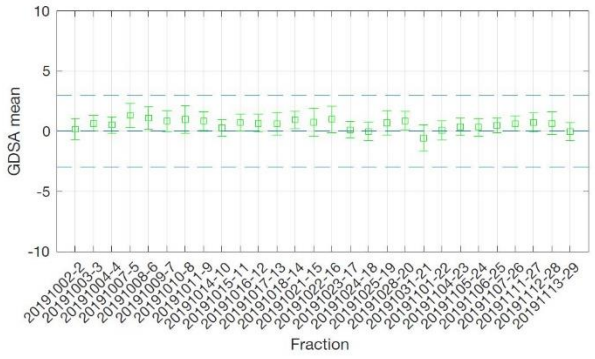

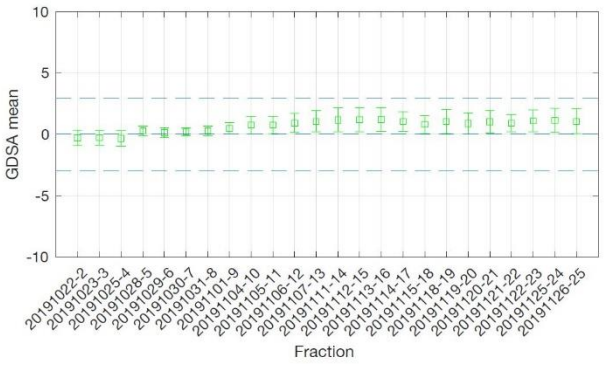

C9 – Cancers of the nervous system

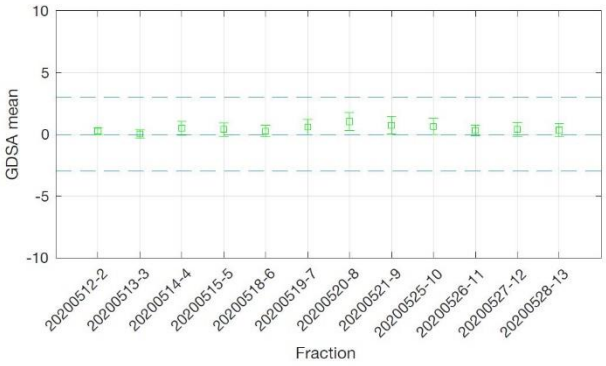

C10 – Orbital cancers

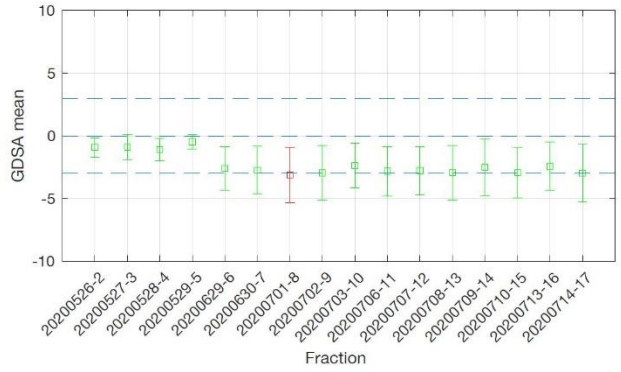

C11 – Oropharyngeal (p16-) cancers

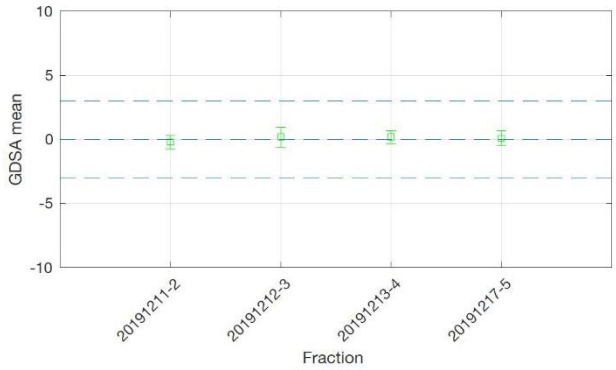

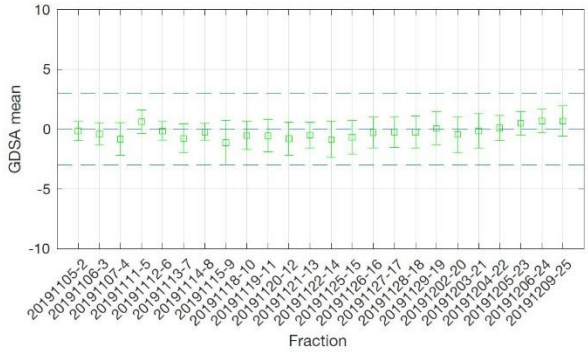

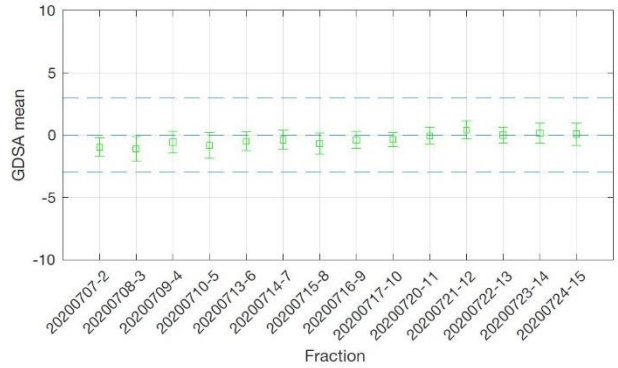

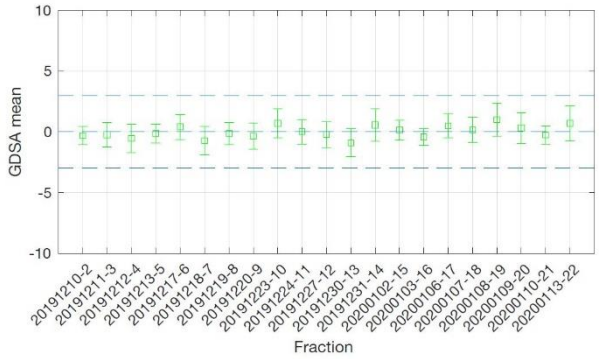

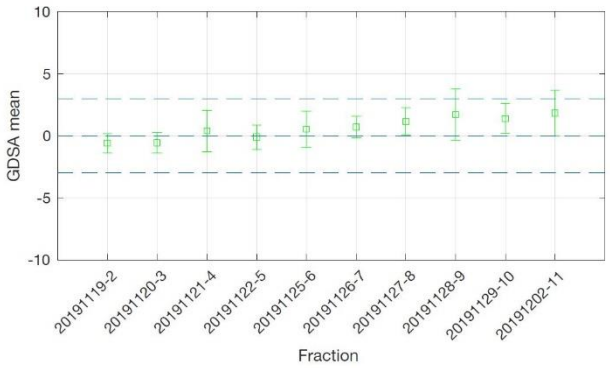

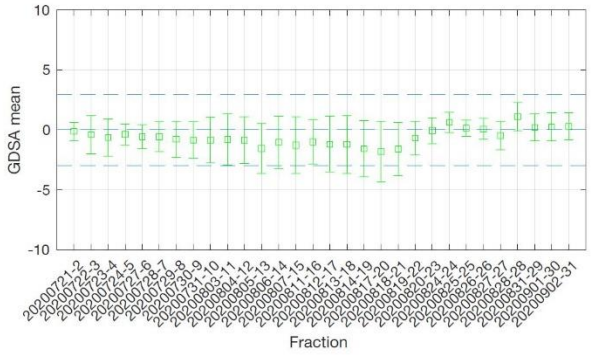

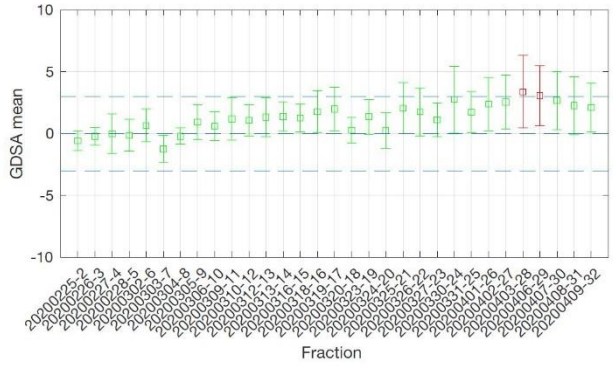

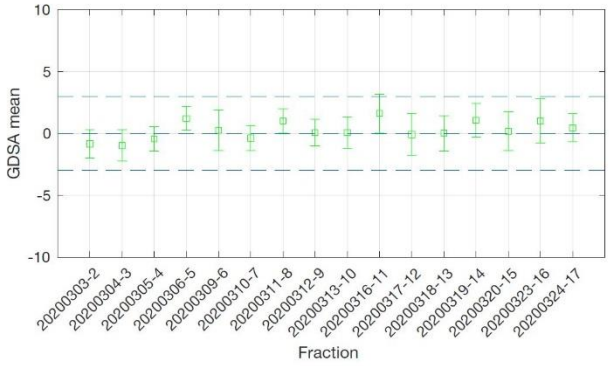

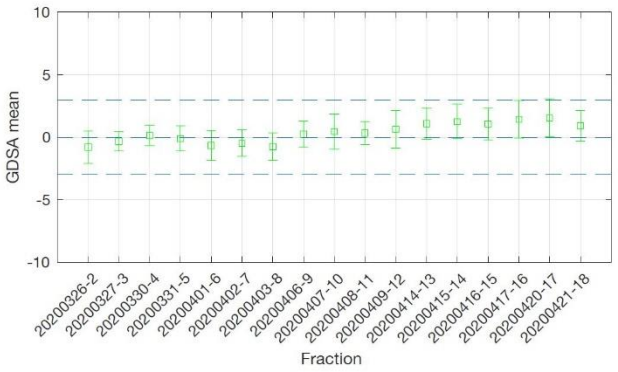

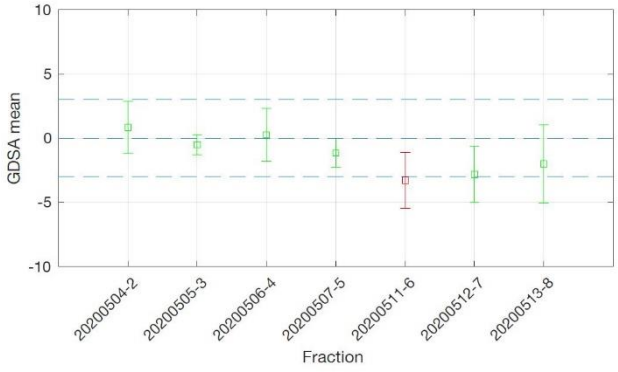

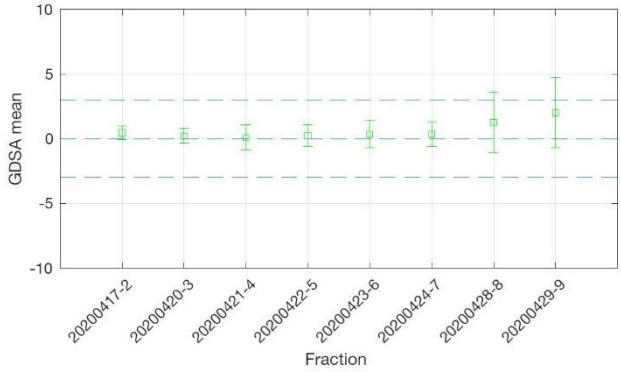

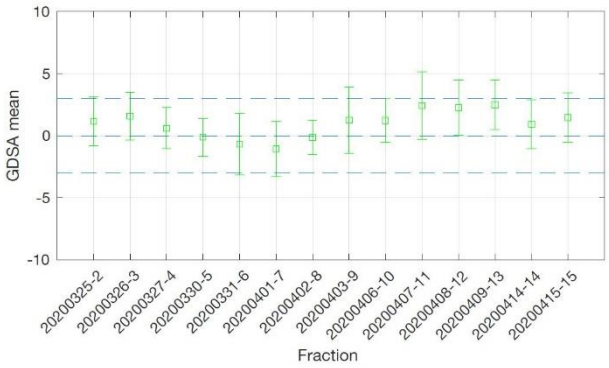

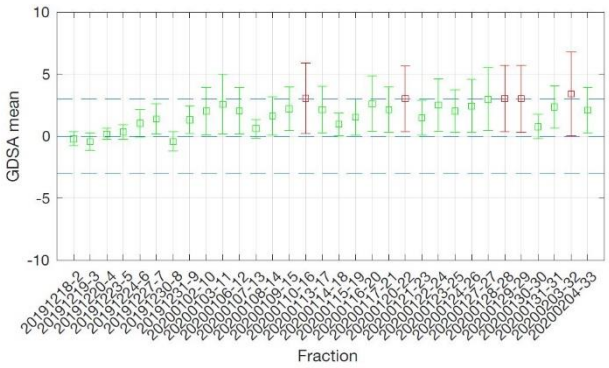

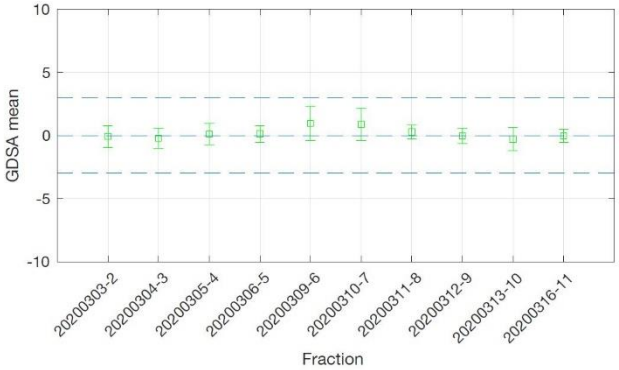

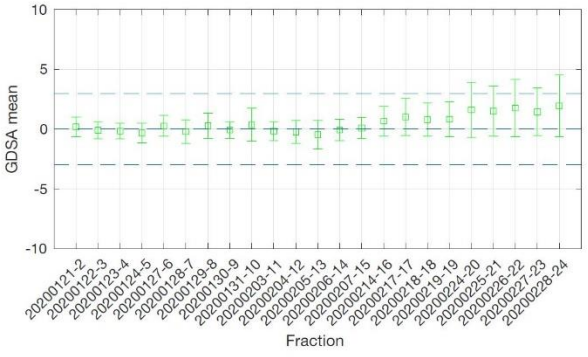

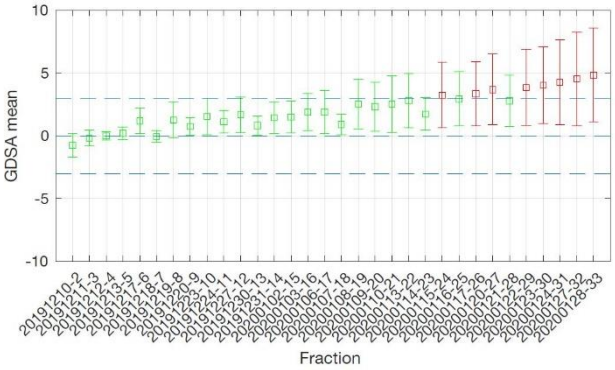

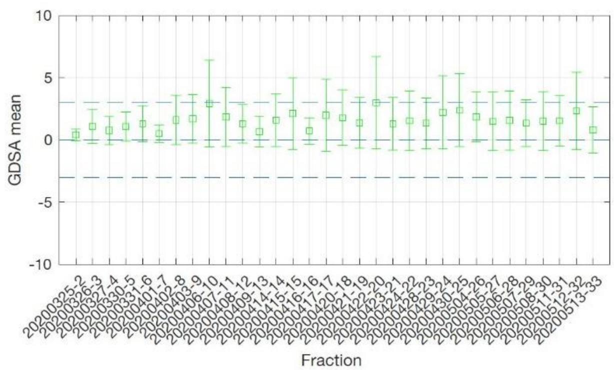

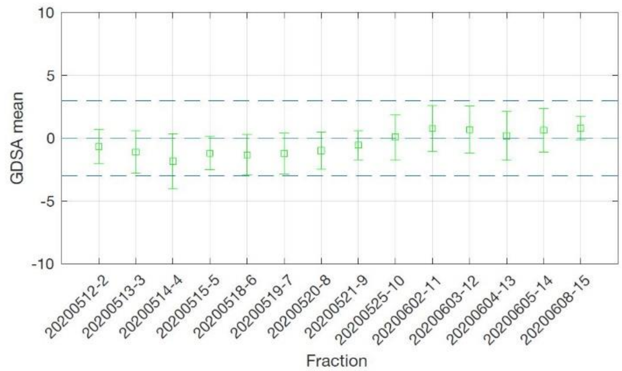

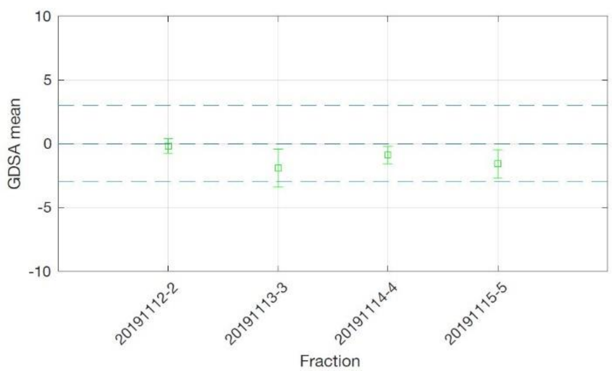

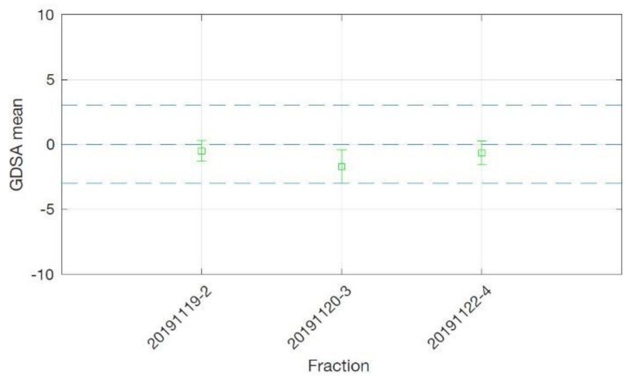

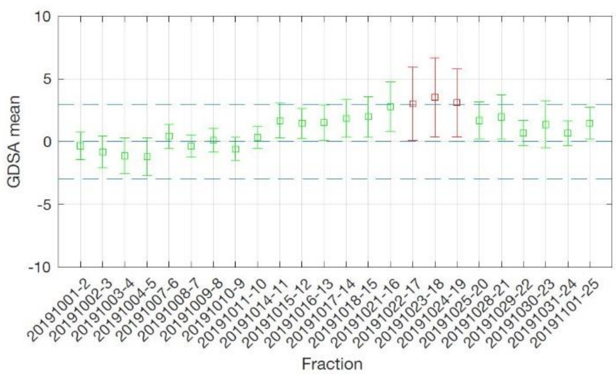

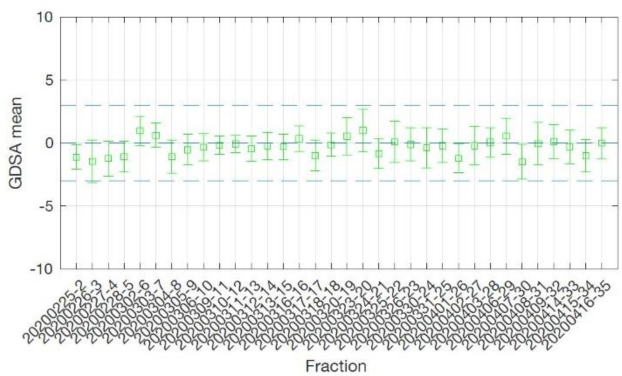

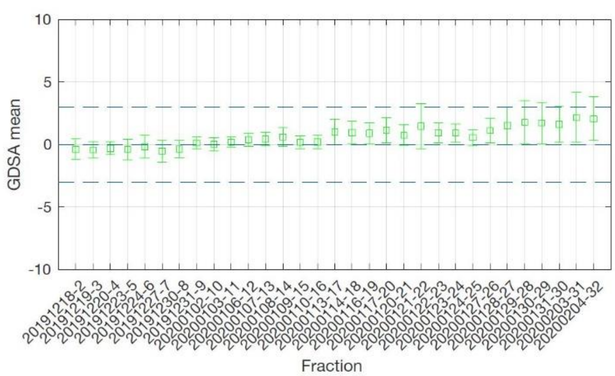

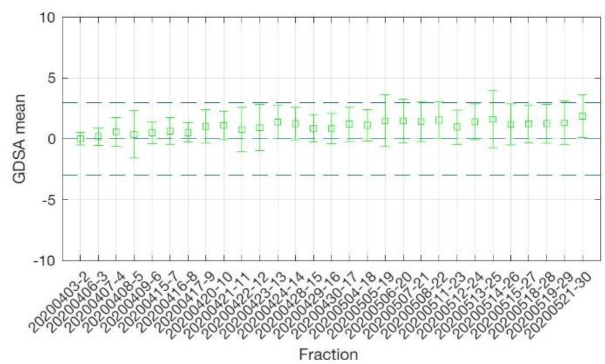

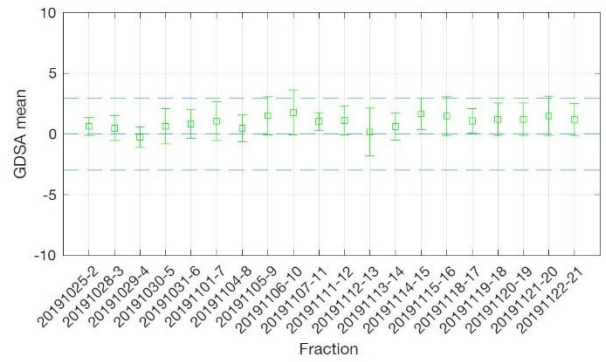

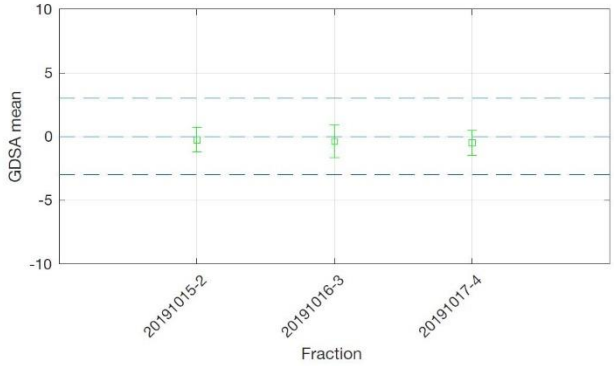

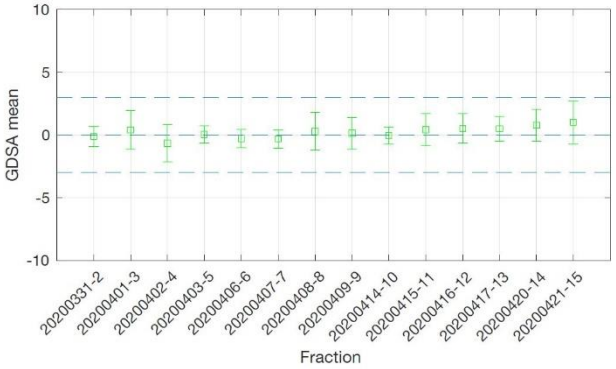

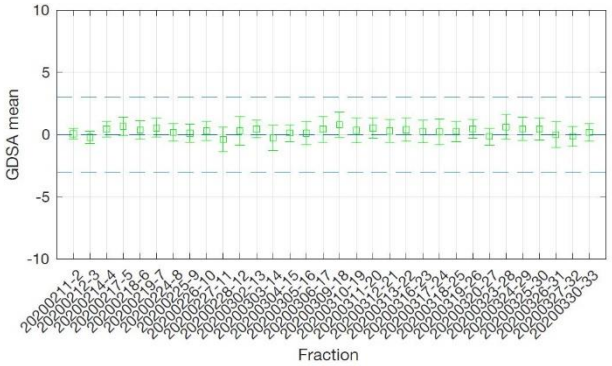

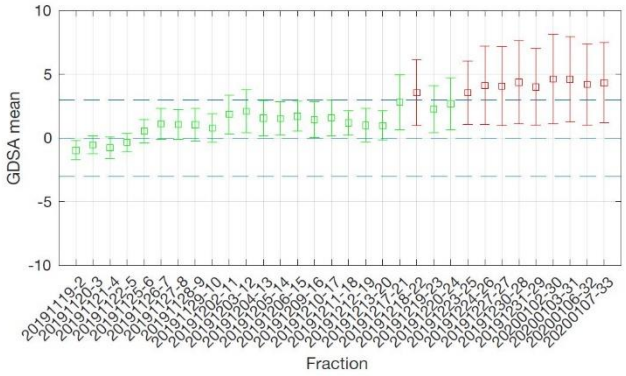

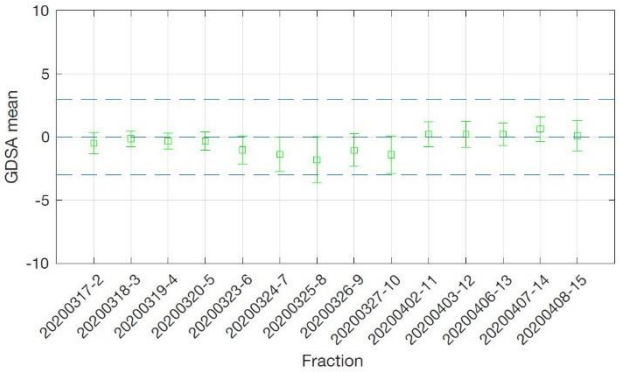

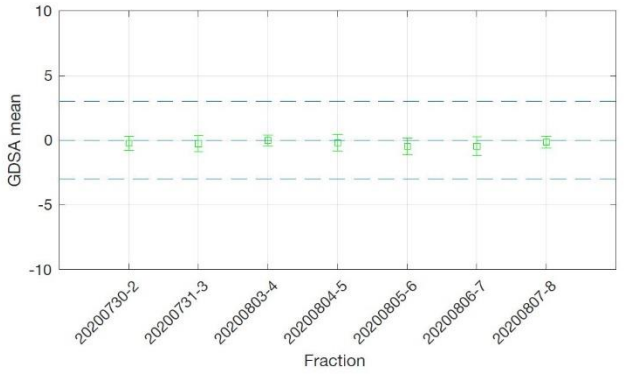

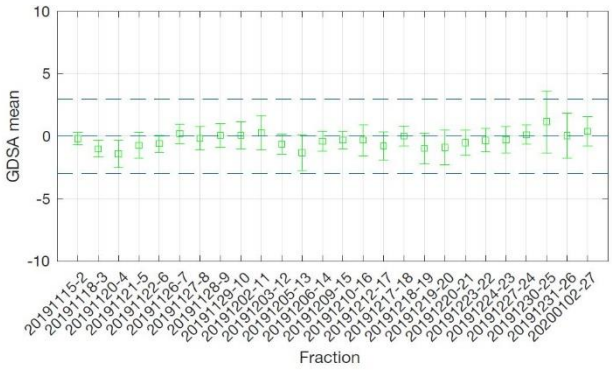

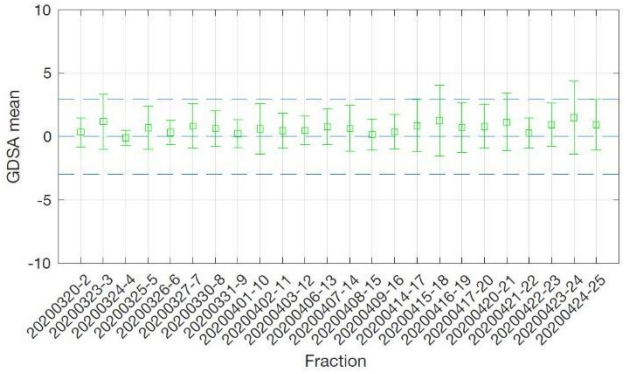

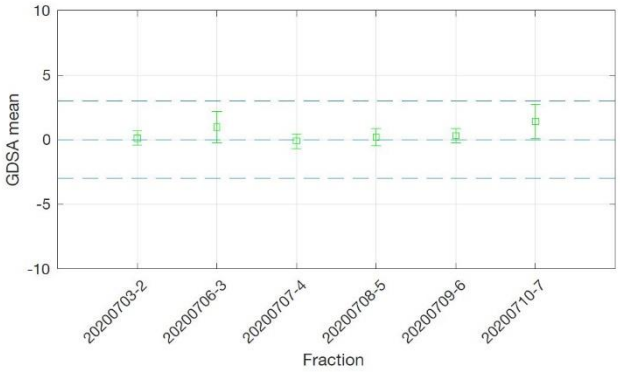

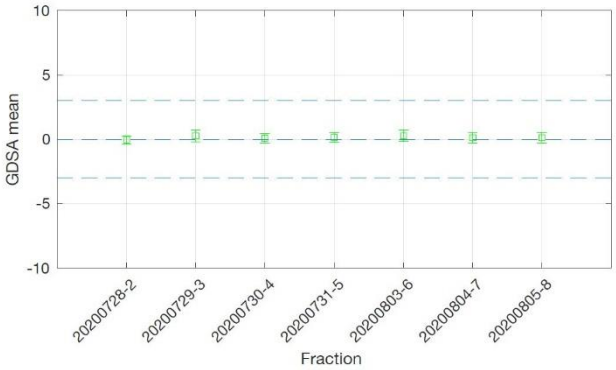

C12 – Salivary gland cancers

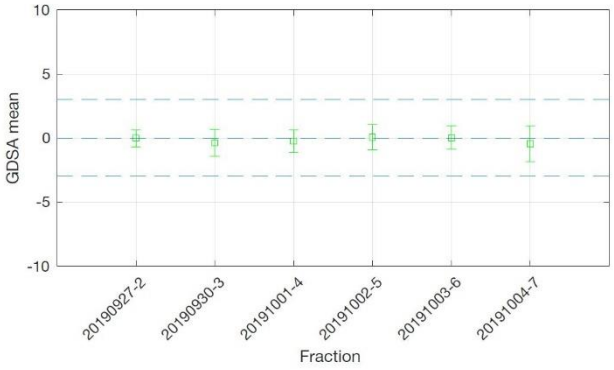

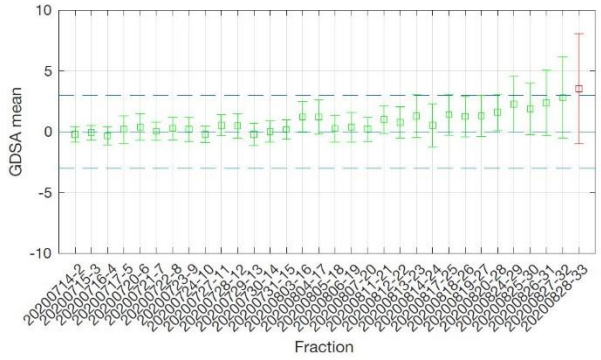

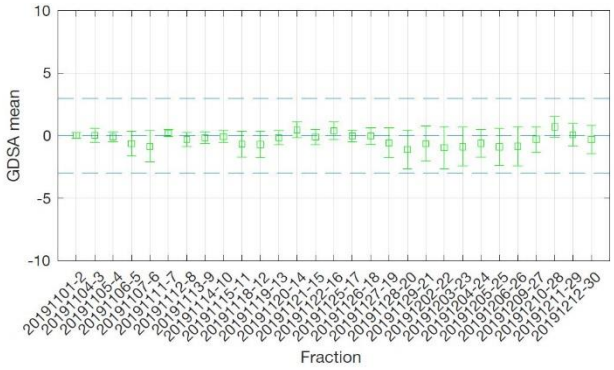

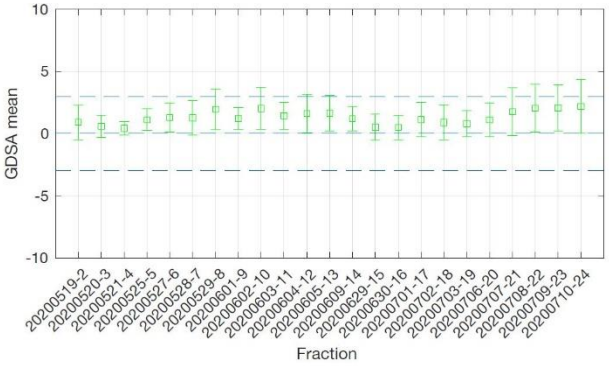

C13 – Thyroid gland cancers